Theoretical Population Biology **56**, 243–263 (1999)
Article ID tpbi.1999.1431, available online at http://www.idealibrary.com on IDEAL®

Competition and Dispersal in Predator–Prey Waves

Nicholas J. Savill[1] and Paulien Hogeweg

Theoretical Biology and Bioinformatics, Utrecht University, Padualaan 8, 3584 CH Utrecht, The Netherlands

E-mail: N.J.Savill@hw.ac.uk

Received March 20, 1998

Dispersing predators and prey can exhibit complex spatio-temporal wave-like patterns if the interactions between them cause oscillatory dynamics. We study the effect of these predator–prey density waves on the competition between prey populations and between predator populations with different dispersal strategies. We first describe 1- and 2-dimensional simulations of both discrete and continuous predator–prey models. The results suggest that any population that diffuses faster, disperses farther, or is more likely to disperse will exclude slower diffusing, shorter dispersing, or less likely dispersing populations, everything else being equal. It also appears that it does not matter whether time, space, or state are discrete or continuous, nor what the exact interactions between the predators and prey are. So long as waves exist the competition between populations occurs in a similar fashion. We derive a theory that qualitatively explains the observed behaviour and calculate approximate analytical solutions that describe, to a reasonable extent, these behaviours. Predictions about the cost of dispersal are tested. If strong enough, cost can reverse the populations' relative competitive strengths or lead to coexistence because of the effect of spiral wave cores. The theory is also able to explain previous results of simulations of coexistence in host–parasitoid models (Comins, H. N., and Massell, M. P., 1996, *J. Theor. Biol.* 183, 19–28).

Key Words: **spatial pattern formation; oscillations; individual oriented models; spiral waves; turbulence.**

1. INTRODUCTION

Dispersal is a ubiquitous phenomenon in the natural world. Its importance in understanding the ecological and evolutionary dynamics of populations is mirrored by the large number of mathematical models devoted to it in the scientific literature (for a detailed review see Johnson and Gaines, 1990; more recent work includes Gustafson and Gardner, 1995; Johst and Brandl, 1997). The general conclusion from the theoretical work indicates that temporal variation tends to result in increased dispersal and spatial variation in decreased dispersal (Johnson and Gaines, 1990; McPeek and Holt, 1992). There are, of course, some exceptions: for example, Hamilton and May (1997), who looked at competitive interactions among relatives, and Johst and Brandl (1997), who looked at the temporal order of reproduction and dispersal. In this paper we will consider only unconditional dispersal of asexually reproducing populations.

The previous work on the evolution of dispersal almost invariably makes use of multi-patch models where organisms that do disperse can disperse into any of the available patches. This assumes that all patches are within reach from any other patch and that the cost of reaching a patch from any other is identical. This is not

[1] To whom correspondence should be addressed. Current address: Department of Mathematics, Heriot-Watt University, Edinburgh EH14 4AS, United Kingdom.

0040-5809/99 $30.00

true for many species, where their range may extend over more area than any one organism can visit in its lifetime (Wright, 1943). In this paper we study what effect this has on competing populations with different dispersal strategies with the help of so-called spatially extended (or explicit) models (Hogeweg, 1988; Durrett and Levin, 1994; Holmes *et al*., 1994).

Another assumption used in previous work is that the spatial heterogeneity and the temporal fluctuations are exogenous, i.e., they are forced upon the populations within each patch. It can be the case, however, that the interactions between dispersing populations induce spatial heterogeneity and/or temporal fluctuations through so-called self-structuring without help from external forcing, i.e., the patterns are endogenous. There are several processes that can lead to the formation of these spatial and temporal patterns (Turing, 1952; Cross and Hohenberg, 1993). We will consider one, namely self-oscillation. This occurs frequently in ecological models of predator and prey interactions and we will use these models to study competition in spatially extended oscillatory systems.

Theoretical work has shown that spatial and temporal pattern formation can play a very important role in ecological and evolutionary systems. Patterns can affect, for example, stability of ecosystems (Hassell *et al*., 1991; McCauley *et al*., 1996; Bascompte and Solé, 1996), the coexistence of species (Solé *et al*., 1992; Ruxton and Rohani, 1996), invasion of mutants (Boerlijst and Hogeweg, 1991b), and chaos (Ruxton, 1996). Moreover, the patterns themselves may interact, leading to selection on the level of patterns (Boerlijst and Hogeweg, 1991a; Boerlijst *et al*., 1993; Savill *et al*., 1997), interlocking eco-evolutionary time scales (van der Laan and Hogeweg, 1995), evolutionary stagnation (Savill and Hogeweg, 1997), and diversity (Hogeweg, 1994).

In spatial oscillatory systems typical patterns include spiral waves, turbulence, and target patterns. Much theoretical work is devoted to this area because of its wide applications in physics. The overwhelming majority of this theory concerns continuous systems (continuous in time, space, and state). However, there is a growing body of literature on the simulation of discrete systems (discrete in time and/or space and/or state) that shows that the patterns mentioned above are generic to all oscillatory systems (e.g., Solé and Valls, 1992; Sherratt *et al*., 1997). At this time though there is no formal theory that proves the link between continuous and discrete systems. If the patterns are generic then it is probable that they influence the ecological and evolutionary dynamics of both continuous and discrete systems in a similar fashion. In this paper we give an intuitive argument for why this is so for competition in any oscillatory system. We also show several simulations and develop theories in continuous and discrete time systems (space and state continuous) that shows that this is indeed true for the competition between populations with different dispersal strategies.

As a starting point for the simulations and theory we assume there is no cost to dispersing, the reason being that cost can come in many forms and strengths and adds an extra parameter to the models. We first examine the ecological dynamics without cost to see what possible behaviours the models can exhibit. Cost is then added to see what possible effects this has on the models.

The paper is organised as follows: In the next section we describe the numerous simulations of both continuous and discrete predator–prey models. This is done to show that the patterns generated by these models are generic and their effect on the ecological dynamics are similar. In each simulation we have two competing prey populations and two competing predator populations. Predator–prey interactions are used primarily to achieve spatio-temporal oscillations but also to demonstrate the generality of competition between differently dispersing populations with oscillatory dynamics.

In the Theory section we derive theories for continuous and discrete time systems that predict the behaviour seen in the simulations. The theory is not meant to be rigorous; we wish to keep the mathematics simple so that the essence of the ideas is clear and concise. Comparisons between the results of the simulations and the theory are shown and several predictions are made and tested.

2. SIMULATIONS

2.1. Introduction

In this section we will show simulations of continuous and discrete spatially extended predator–prey models exhibiting waves. The first two simulations are 1- and 2-dimensional models of predator–prey interactions with continuous time, space and state and are modelled as partial differential equations (PDE). The equations are of the reaction–diffusion type. These equations have a set of reaction terms that model the predator–prey interactions and diffusion terms that model dispersal.

The next two simulations are 1- and 2-dimensional models of host–parasitoid interactions (formally equivalent to predator–prey interactions) with continuous state and discrete time and space and are modelled as coupled map lattices (CML). These are discrete generation models

where, within one generation, the hosts and parasitoids first disperse and then interact.

The final two simulations are 2-dimensional models of a continuous time predator–prey system and a discrete time host–parasitoid system both with discrete space and discrete individuals (states), i.e., individual oriented (IO) models. In these models individuals are modelled as separate entities as opposed to modelling local densities as in the continuous state PDE and CML models.

In all of the simulations we have two prey (host) populations that compete and two predator (parasitoid) populations that compete. There is no competition between the predator and prey populations; we only utilise the interactions between them to get oscillatory dynamics. The competing populations are identical in every respect except for their dispersal strategies. In the PDE models the competing populations have different diffusion coefficients; in the CML and IO models the competing populations have different maximum dispersal distances.

The models can also be interpreted as the invasion of a mutant with a different dispersal distance or diffusion coefficient into a wildtype population. Although the initial conditions would be different from those in the simulations, our major conclusions would still hold.

2.2. 1D PDE Predator–Prey Simulation

The system we use is the well-known Lotka–Voltera model with self-limitation of the prey and Holling type II functional response for two prey and two predator populations,

$$\dot{r}_i(x, t) = \left(a - br - \frac{p}{1+r}\right) r_i + d_{r_i} \nabla^2 r_i \qquad (1)$$

$$\dot{p}_i(x, t) = \left(\frac{r}{1+r} - c\right) p_i + d_{p_i} \nabla^2 p_i, \qquad (2)$$

where t and x represent time and space, $r = r_1 + r_2$ and $p = p_1 + p_2$, a, b, and c are positive parameters, and d_{r_i} and d_{p_i} are the diffusion coefficients of the prey and predator populations, respectively. The system has already been normalised. The values of the parameters are chosen so that the system exhibits oscillations (i.e., in the spatially homogeneous case the attractor is a stable limit cycle). Both prey populations and both predator populations are identical in every respect except for their diffusion coefficients which are $d_{r_1} = d_{p_1} = 0.5$ and $d_{r_2} = d_{p_2} = 1$.

Figure 1a shows a space–time plot of a typical simulation. Time runs from top to bottom. From left to right we have r_1, r_2, p_1, and p_2. The length of the 1-dimensional space is 200 length units. The initial condition is one predator–prey wave of wavelength 200 length units. The initial densities are $r_1 = 9r_2$ and $p_1 = 9p_2$ at all positions. Space has periodic boundary conditions so that as the wave travels off the right of space it reappears on the left. The simulation clearly shows that the faster diffusing prey and predator populations (r_2 and p_2) exclude the slower diffusing populations (r_1 and p_1).

Figure 1b shows the proportion of each population at a certain point in space. In the top plot we show the proportion of the two prey populations (thick line $r_1/(r_1 + r_2)$, thin line $r_2/(r_1 + r_2)$). In the bottom plot we show the proportion of the two predator populations (thick line $p_1/(p_1 + p_2)$, thin line $p_2/(p_1 + p_2)$). Notice the sigmoid shape of the curves in both plots.

2.3. 2D PDE Predator–Prey Simulation

This simulation is similar to the 1D simulation. The only differences between the two are zero flux instead of periodic boundary conditions and complex spatial patterns of spirals and turbulence instead of one plane wave as initial conditions. The boundary conditions have been changed from the 1D simulation to demonstrate that they have no qualitative effect on the competitive dynamics. All other parameters and initial densities are the same.

The system is allowed to evolve freely exhibiting complex spatio-temporal patterns instead of the stable plane wave in the 1D simulation (Fig. 2a). Again, the faster diffusing populations exclude the slower diffusing populations. The first thing to notice is that, at a given point in space, the amplitude of the oscillations varies in a complex fashion (Fig. 2b). This is because the spatial patterns shift and change over time. This is a well-known effect in spatial oscillatory systems. Typically, at a given point in space either spirals or turbulence can be observed. Turbulence, by its very nature, exhibits varying amplitudes and wavelengths. Spirals, on the other hand, are highly structured. A spiral is composed of a core and an arm. At the centre of the core is a singular defect that has zero amplitude oscillations. Moving radially away from the defect the amplitude increases (the core) until it saturates in the arm of the spiral. Where waves collide, at so-called shocks, the amplitude shows a small increase.

Figure 2c shows the change in the predator and prey proportions at a point in space. Note that the proportions oscillate at the same frequency as the predator and prey densities. The oscillations give us a handle with which to calculate the rate of exclusion of the slower diffusing population by the faster diffusing population.

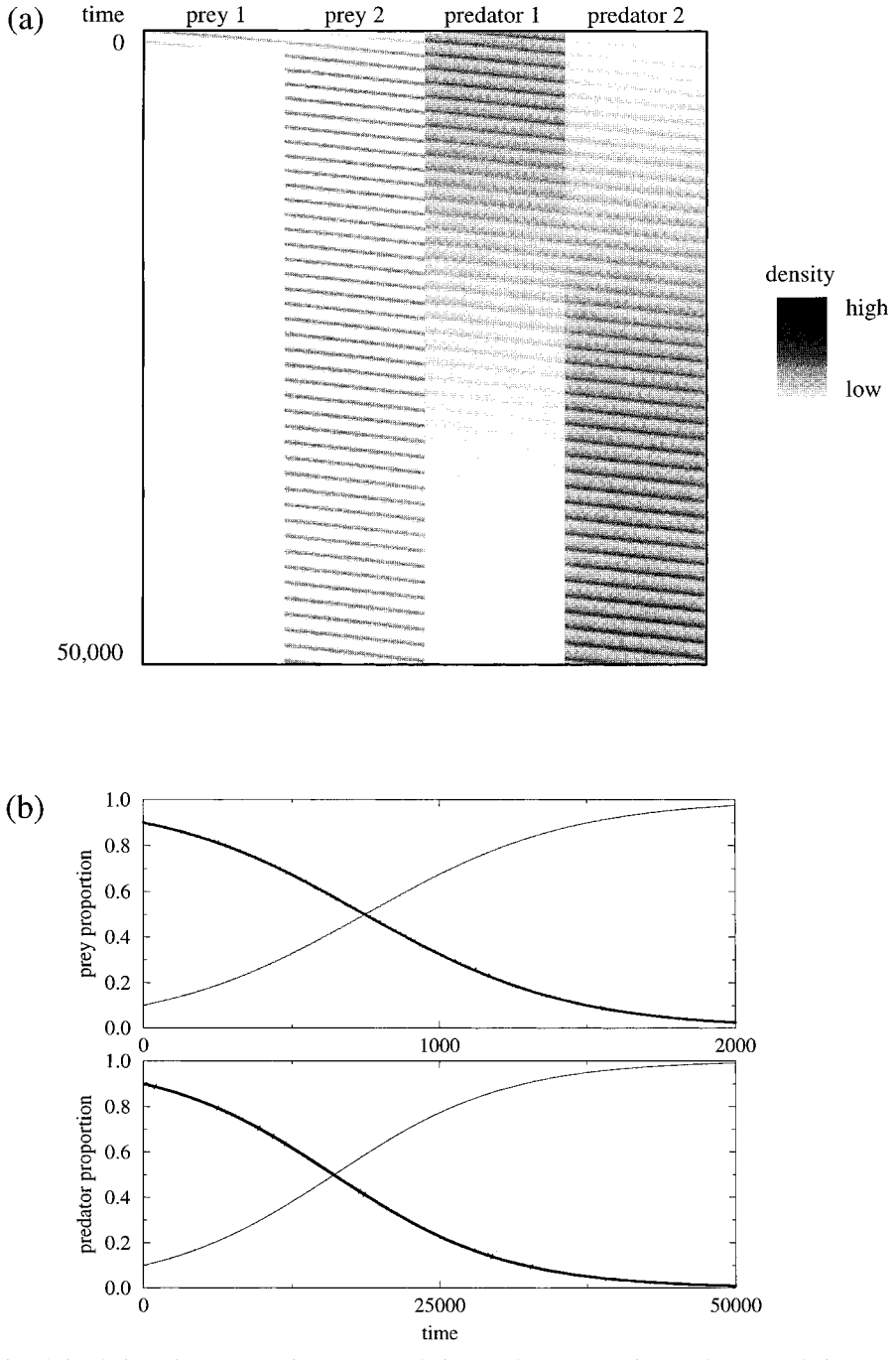

FIG. 1. One-dimensional simulation of two competing prey populations and two competing predator populations modelled using the Lotka–Voltera system with self-limitation of the prey and Holling type II functional response given by Eqs. (1) and (2). Both prey populations and both predator populations are identical except for their diffusion coefficients, $d_{r_1} = d_{p_1} = 0.5$ and $d_{r_2} = d_{p_2} = 1$. The 1-dimensional space has a length of 200 space units and has periodic boundary conditions. The initial condition is one wave covering the whole space and has been allowed to run to remove transients. The initial densities are $r_1 = 9r_2$ and $p_1 = 9p_2$. The parameters are $a = 2.2$, $b = 1.1$, and $c = 0.18$. The integration scheme is FTCS with $\delta_t = 0.01$ and $\delta_x = 0.3$. δ_x was chosen so that the smallest wavelength, found by observation, spanned approximately five lattice points. δ_t was then chosen so that the solution was within stability limits, i.e., $4d\delta_t/\delta_x^2 \leqslant 1$. (a) Space–time plot of the simulation with time running from top to bottom from 0 to 50,000 time units, plotted every 50 time units. From left to right we plot the population densities of r_1, r_2, p_1, and p_2. The faster diffusing prey and predator populations exclude the slower diffusing populations. The competition between the prey is much stronger. Note that the frequency of the waves is much higher than that depicted in the figure. (b) The proportion of each population over time at a certain point in space. Top plot shows the prey (thick line ρ_{r_1}, thin line ρ_{r_2}), bottom plot the predators (thick line ρ_{p_1}, thin line ρ_{p_2}).

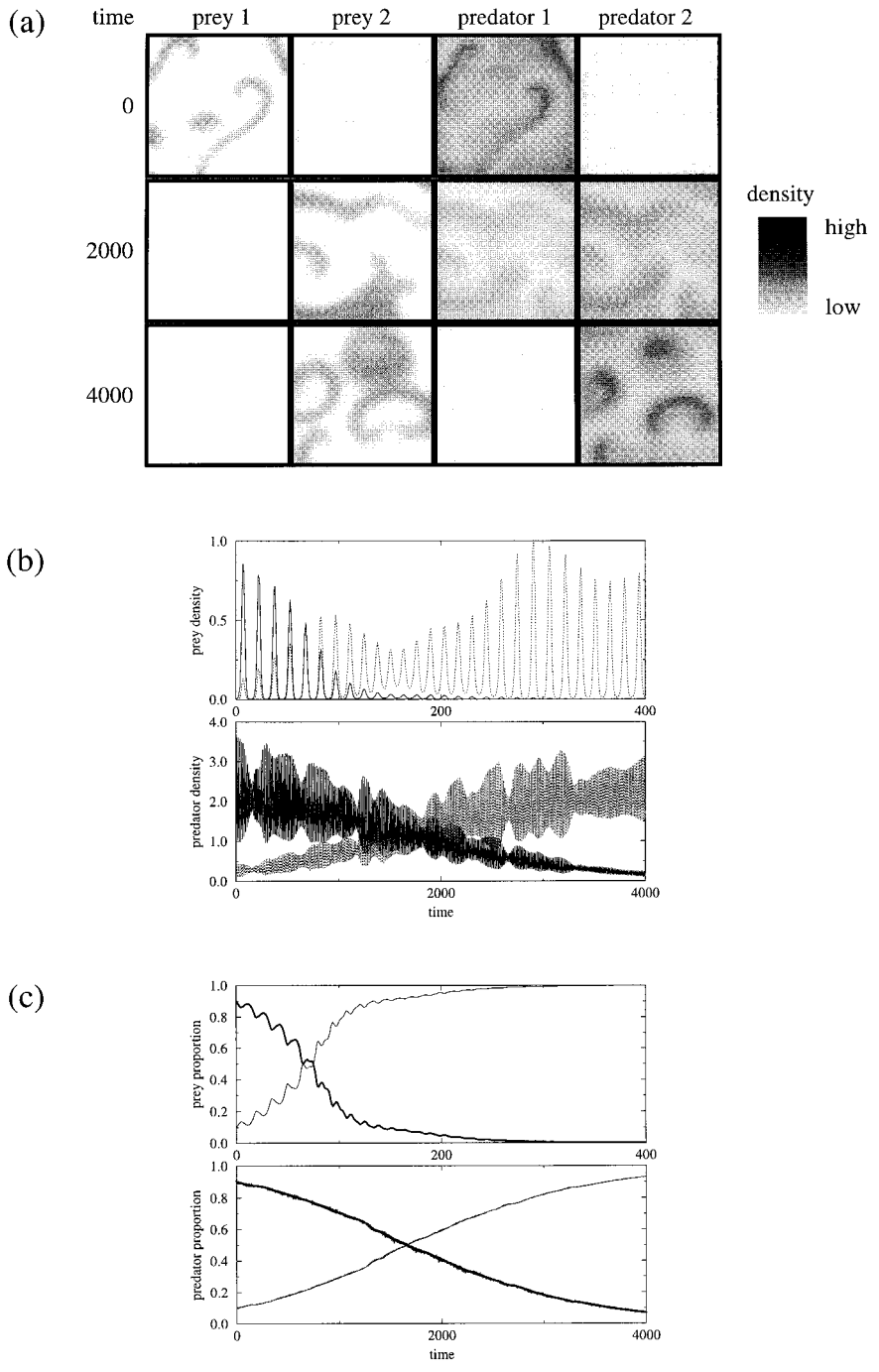

FIG. 2. Two-dimensional simulation of two competing prey populations and two competing predator populations similar to Fig. 1. Space is 100×100 space units and has zero flux boundary conditions. The initial condition has been allowed to run to remove transients and is a complex pattern of spirals and turbulence. The integration scheme is Crank–Nicholson with $\delta_t = 0.1$ and $\delta_x = 0.3$. δ_x was chosen in a fashion similar to that for Fig. 1. δ_t was chosen to provide sufficient temporal resolution. Parameters and initial population densities are the same as in Fig. 1. (a) Three snapshots showing the faster diffusing predator and prey populations excluding the slower diffusing populations. The competition between the prey is much stronger. (b) The two prey (top) and two predator (bottom) population densities at a given point in space (r_1 and p_1 solid lines, r_2 and p_2 dotted lines). There are complex temporal fluctuations as the spatial patterns shift and change over time. (c) The proportion of each population over time at a certain point in space. Top plot shows the prey (thick line ρ_{r_1}, thin line ρ_{r_2}), bottom plot the predators (thick line ρ_{p_1}, thin line ρ_{p_2}). The oscillations in the proportions are due to the differential flow rates of prey and predators from high densities regions to low densities regions. They occur in all simulations but may be difficult to see because of very long time scales.

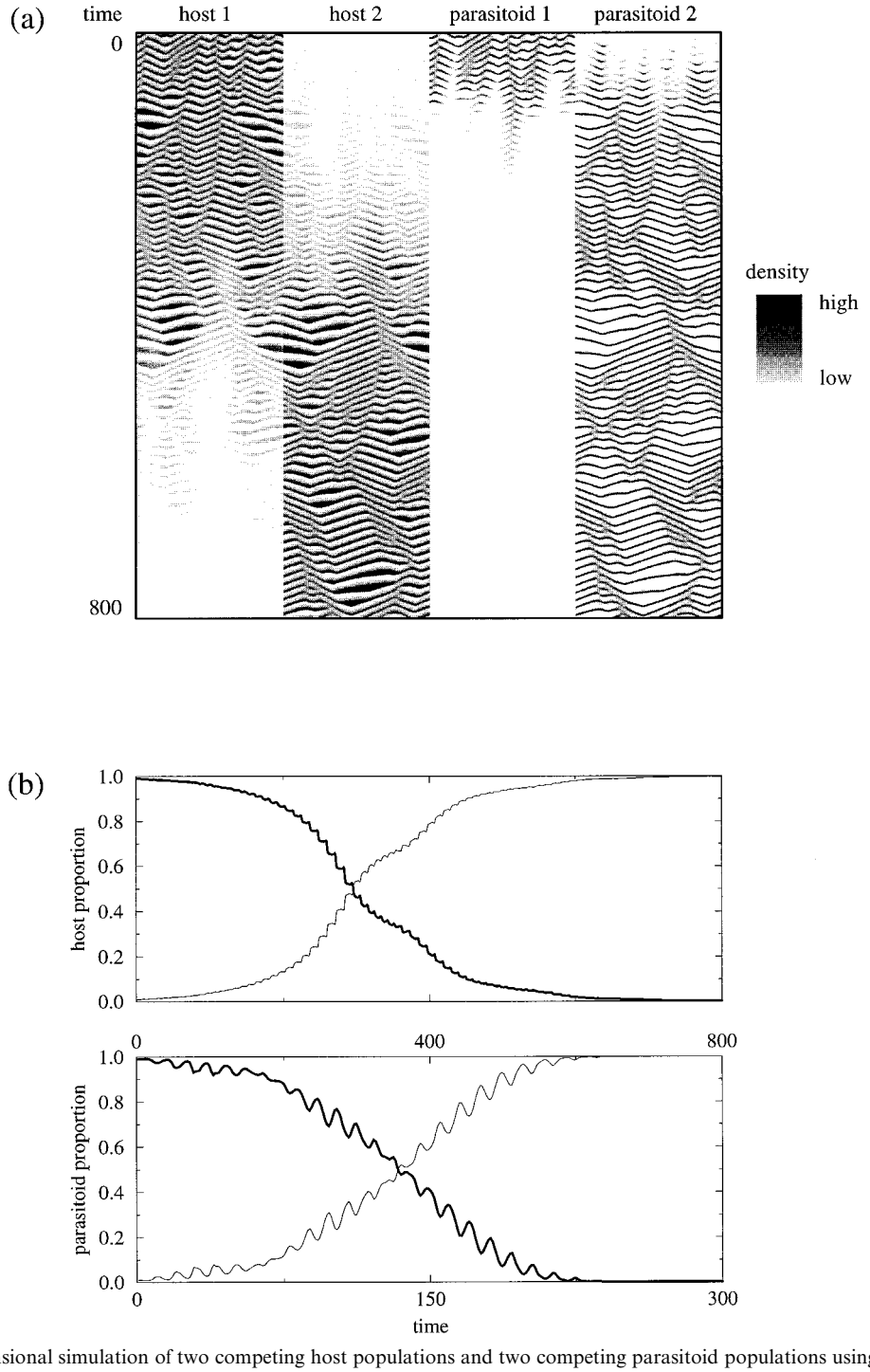

FIG. 3. One-dimensional simulation of two competing host populations and two competing parasitoid populations using the Nicholson–Bailey equations with self-limitation of the hosts. The competing populations are identical except for their maximum dispersal distances, which are $d_{r_1} = d_{p_1} = 2$ and $d_{r_2} = d_{p_2} = 3$. Space is 200 patches wide and has periodic boundary conditions. The initial condition has been allowed to run to remove transients and is a complex pattern of defects, waves, and shocks. The initial densities are $r_1 = 99r_2$ and $p_1 = 99p_2$. The parameters are $a = 2$, $b = 300$, $c = 0.05$, $d = 1$, $\alpha_r = 0.2$, and $\alpha_p = 0.9$. (a) Space–time plot of the simulation with time running from top to bottom from 0 to 800 generations, plotted every generation. From left to right we plot the population densities of r_1, r_2, p_1 and p_2. The farther dispersing host and parasitoid populations exclude the shorter dispersing populations. The competition between the parasitoids is much stronger than that between the hosts. Competition is strong in shocks where waves collide and weak in defects (cores). (b) The proportion of each population over time at a certain point in space. Top plot shows the hosts (thick line ρ_{r_1}, thin line ρ_{r_2}), bottom plot the parasitoids (thick line ρ_{p_1}, thin line ρ_{p_2}).

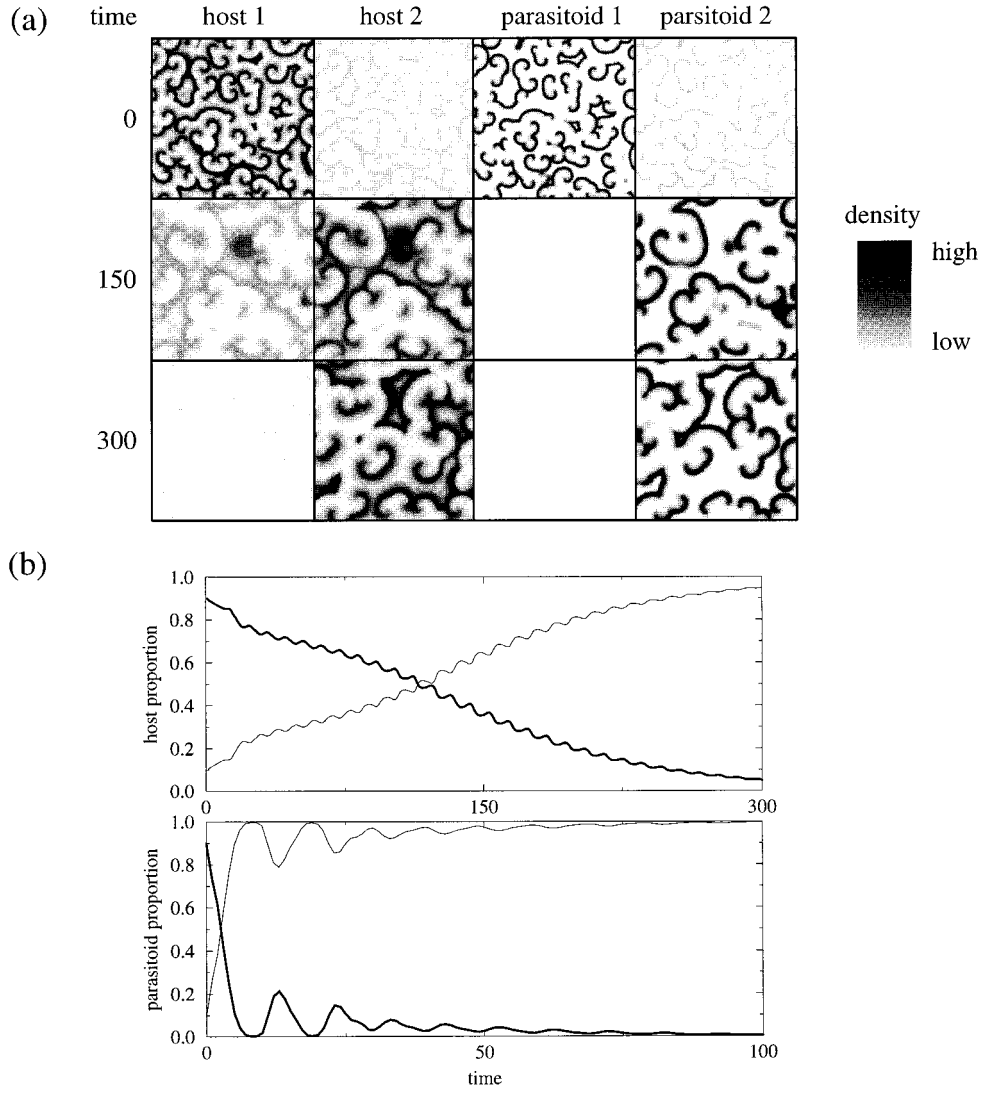

FIG. 4. Two-dimensional simulation of two competing host populations and two competing parasitoid populations similar to Fig. 3. The maximum dispersal distances are $d_{r_1} = d_{p_1} = 1$ and $d_{r_2} = d_{p_2} = 2$. Space is a square lattice of 150×150 patches and has periodic boundary conditions. The initial condition has been allowed to run to remove transients and is a complex pattern of many spirals. The initial densities are $r_1 = 9r_2$ and $p_1 = 9p_2$. The parameters are the same as in Fig. 3. (a) Three snapshots showing the farther dispersing hosts and parasitoids excluding the shorter dispersing populations. As the farther dispersing populations win the size of the patterns increases. (b) The proportion of each population over time at a certain point in space. Top plot shows the hosts (thick line ρ_{r_1}, thin line ρ_{r_2}), bottom plot the parasitoids (thick line ρ_{p_1}, thin line ρ_{p_2}).

2.4. 1D and 2D CML Host–Parasitoid Simulations

These simulations are based on models developed by Hassell *et al.* (1991) and Comins *et al.* (1992). Time is discretised into generations. In each generation there is first dispersal of hosts and parasitoids then parasitism and reproduction. Space is also discretised into a lattice of square patches. Hosts and parasitoids may randomly disperse from one patch to another local patch. If $r_i(\mathbf{x}, t)$ and $p_i(\mathbf{x}, t)$ are the host and parasitoid pre-dispersal densities at time t then $r'_i(\mathbf{x}, t)$ and $p'_i(\mathbf{x}, t)$ are the post-dispersal densities given by

$$r'_i(\mathbf{x}, t) = (1 - \alpha_r)\, r_i(\mathbf{x}, t) + \alpha_r \int_{-\infty}^{\infty} r_i(\mathbf{x} - \xi, t)\, D_{r_i}(\xi)\, d\xi \tag{3}$$

$$p'_i(\mathbf{x}, t) = (1 - \alpha_p)\, p_i(\mathbf{x}, t) + \alpha_p \int_{-\infty}^{\infty} p_i(\mathbf{x} - \xi, t)\, D_{p_i}(\xi)\, d\xi, \tag{4}$$

where α_r and α_p are the dispersal probabilities of hosts and parasitoids, respectively. The first terms in Eqs. (3) and (4) represent those hosts and parasitoids that do not disperse, the second terms those that do. The functions D_{r_i} and D_{p_i} describe the dispersal distribution of hosts and parasitoids from a given patch. For example, they might have a Gaussian distribution. In these simulations we use a flat distribution; e.g., in 2D,

$$D_{r_i}(\mathbf{x}) = \begin{cases} \dfrac{1}{\pi d_{r_i}^2} & \text{if} \quad \|\mathbf{x}\| \leqslant d_{r_i} \\ 0 & \text{otherwise} \end{cases} \tag{5}$$

$$D_{p_i}(\mathbf{x}) = \begin{cases} \dfrac{1}{\pi d_{p_i}^2} & \text{if} \quad \|\mathbf{x}\| \leqslant d_{p_i} \\ 0 & \text{otherwise,} \end{cases} \tag{6}$$

where d_{r_i} and d_{p_i} are the maximum dispersal distances of the hosts and the parasitoids, respectively. Numerous simulations lead us to conclude that the exact form of the distribution does not qualitatively influence the competitive interactions between populations. The dispersal distances are $d_{r_1} = d_{p_1} = 2$ and $d_{r_2} = d_{p_2} = 3$ for the 1D simulation and $d_{r_1} = d_{p_1} = 1$ and $d_{r_2} = d_{p_2} = 2$ for the 2D simulation.

Once dispersal has taken place the hosts and parasitoids interact. We use the well known Nicholson–Bailey equations (Nicholson and Bailey, 1935) with the addition of self-limitation of the hosts (Varley and Gradwell, 1963),

$$r_i(\mathbf{x}, t+1) = ar_i'(1-r')\, e^{-p'} \tag{7}$$

$$p_i(\mathbf{x}, t+1) = br'(1-e^{-p'})\,\frac{p_i'}{p'}, \tag{8}$$

where $r' = r_1' + r_2'$ and $p' = p_1' + p_2'$ and a and b are positive parameters. The details of the models are given in the figure legends (Figs. 3 and 4).

For the 1D simulation Fig. 3a shows the space–time plot. The farther dispersing host and parasitoid populations

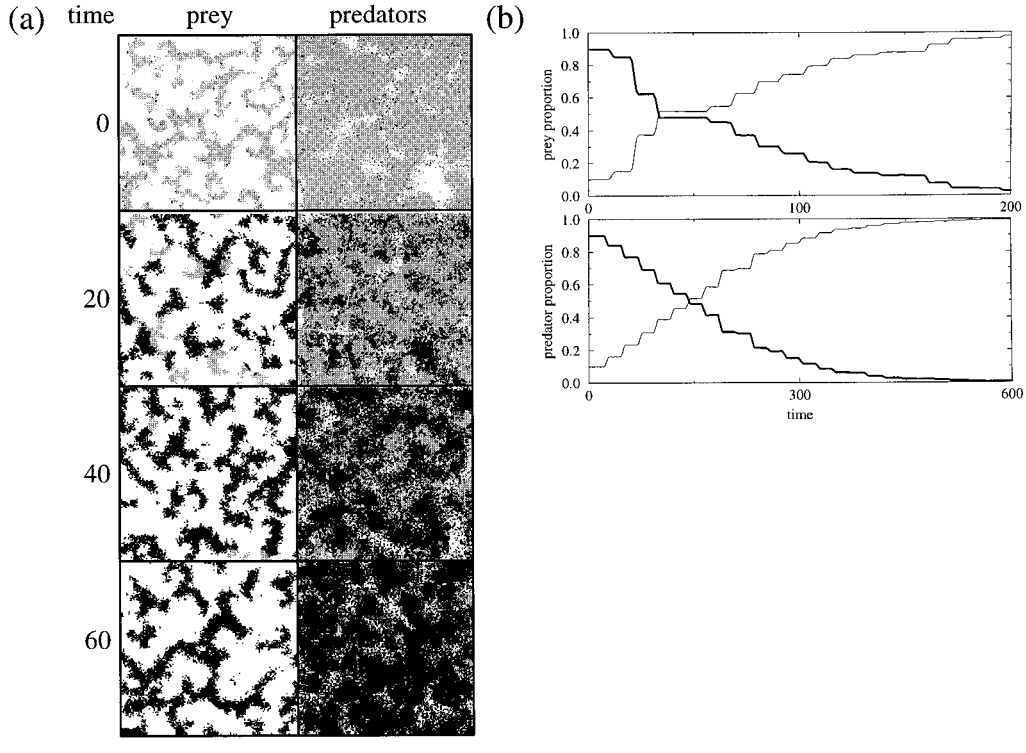

FIG. 5. Two-dimensional simulation of the individual oriented predator–prey model. The competing populations are identical except for their maximum dispersal distances which are $d_{r_1} = d_{p_1} = 2$ and $d_{r_2} = d_{p_2} = 3$. Space is a square lattice of 150×150 patches and has zero boundary conditions. The initial condition has been allowed to run to remove transients and is a complex pattern of spirals and turbulence. The initial densities are $r_1 = 9r_2$ and $p_1 = 9p_2$. (a) Four snapshots showing the farther dispersing predator and prey populations excluding the shorter dispersing populations. We do not plot the competing populations separately as in the continuous state models. Because in each patch there can be many individuals with different dispersal distances we plot the dispersal distance which is in the majority ($d = 2$ light grey, $d = 3$ dark grey, empty patches white). (b) The proportion of each population over time over all space. Top plot shows the prey (thick line ρ_{r_1}, thin line ρ_{r_2}), bottom plot the predators (thick line ρ_{p_1}, thin line ρ_{p_2}).

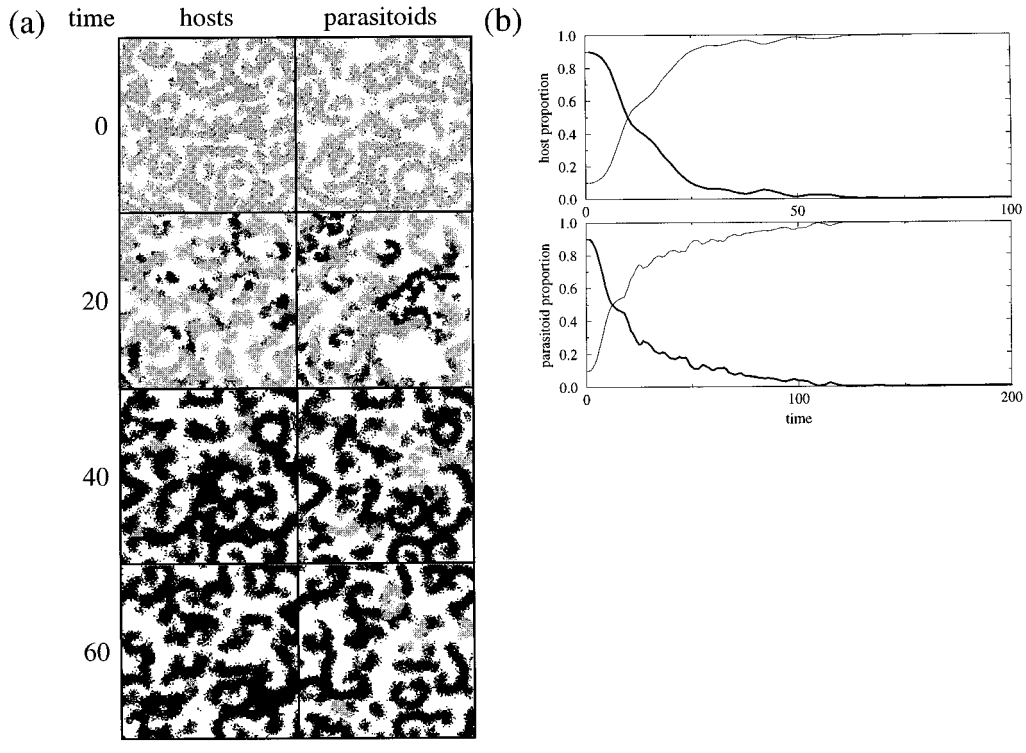

FIG. 6. Two-dimensional simulation of the individual oriented host–parasitoid model. The competing populations are identical except for their maximum dispersal distances which are $d_{r_1} = d_{p_1} = 2$ and $d_{r_2} = d_{p_2} = 3$. Space is a square lattice of 150×150 patches and has zero boundary conditions. The initial condition has been allowed to run to remove transients and is a complex pattern of spirals and turbulence. The initial densities are $r_1 = 9r_2$ and $p_1 = 9p_2$. (a) Four snapshots showing the farther dispersing host and parasitoid populations excluding the shorter dispersing populations (colouring as in Fig. 5). (b) The proportion of each population over time over all space. Top plot shows the hosts (thick line ρ_{r_1}, thin line ρ_{r_2}), bottom plot the parasitoids (thick line ρ_{p_1}, thin line ρ_{p_2}).

exclude the closer dispersing populations. Within defects exclusion occurs more slowly than at shocks where waves collide; this is most easily observed for the parasitoids. Figure 3b shows the proportion of each population at a certain position in space with the characteristic oscillations in the curves. The 2D simulation is shown in Fig. 4 with very similar results. This simulation clearly shows an increase in the size of the spatial patterns as the farther dispersing populations increase in number. This is not really surprising as it is known for diffusive PDE systems that the pattern size increases as the square root of the diffusion coefficient.

2.5. 2D IO Predator–Prey and Host–Parasitoid Simulations

We have also simulated the predator–prey system in continuous time (Fig. 5) and the host–parasitoid system in discrete time (Fig. 6) in IO models to show that using discrete entities gives the same results as for continuous state models. The details of the models are given in the Appendix A.

In both cases the farther dispersing populations always exclude the closer dispersing ones. The size of the spatial patterns increase as the farther dispersing populations increase in numbers. In the previous simulations the proportions of each population were calculated at a single point or patch in space. This is possible because the models have a continuous state and zero densities do not occur. In these discrete state models there may be no individuals in a patch due to local extinctions. Therefore, calculating the proportion in one patch is not very helpful. Thus, the proportion of each population is calculated over the whole of space (Figs. 5b and 6b). This averaging over many waves causes the oscillations in the proportions to become less pronounced.

3. THEORY

3.1. Why Dispersal Confers a Competitive Advantage

If spatial waves exist then diffusion or dispersal will always cause a positive net flux of organisms from the

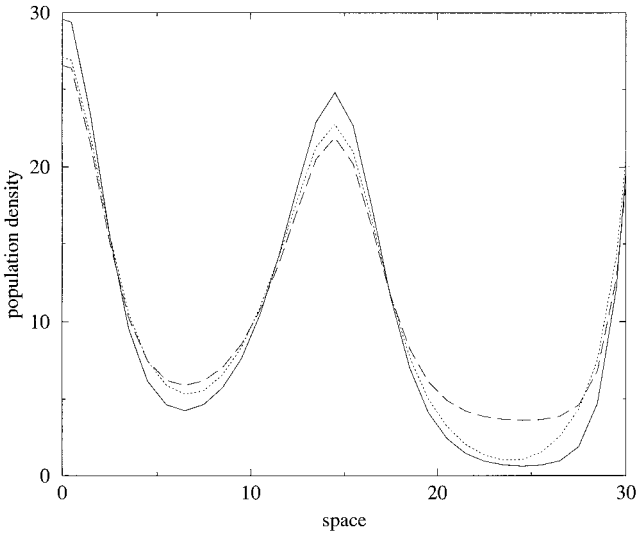

FIG. 7. The host population density before dispersal (solid line) and after dispersal with a dispersal distance of 5 (dotted line) and 15 (dashed line) taken from the 1D CML simulation. More of the farther dispersers disperse into the wave troughs where there is less competition. Hence they have, on average, a higher per-capita growth rate.

peaks into the troughs of the waves (more precisely from regions where $\nabla^2 r < 0$ to regions where $\nabla^2 r > 0$, where r is the population density, Fig. 7). The larger the dispersal the greater the net flux. In the predator–prey systems defined in this paper per–capita growth rates of the populations are a function of the local density. In fact, as the density increases per–capita growth rates decline. This implies that growth rates are larger in the troughs of the waves than in the peaks (Fig. 7). Hence, a population with a larger dispersal distance or diffusion rate with a larger net flux into the wave troughs will have larger per-capita growth rates averaged over the whole wave. Therefore, this population will exclude a population with a smaller dispersal distance or diffusion rate. For example, in Fig. 7 the average per-capita growth rate for the population with $d_r = 5$ (dotted line) is 1.17 and for the population with $d_r = 15$ (dashed line) is 1.35. This would seem to suggest that the faster diffusing population always excludes the slower diffusing population unless the functional form for predator–prey interactions reduces competition as density increases whilst maintaining oscillatory dynamics.

Intuitively one can see that the difference in per-capita growth rates, and hence the rate of exclusion, between the two populations will be some function of the dispersal distances or diffusion rates and the wave amplitude and frequency. In the next section we derive approximate analytical expressions for that function.

3.2. The Oscillations in the Proportions

To formulate an analytical theory for competition in predator–prey waves we will do so in terms of the proportion of each population, namely:

$$\rho_{r_i} = \frac{r_i}{r_1 + r_2} \tag{9}$$

$$\rho_{p_i} = \frac{p_i}{p_1 + p_2}. \tag{10}$$

In the previous section we argued for exclusion by considering competition over the whole wave. To derive analytical expressions we shift the focus into a single point in space. We want to show that the proportion of the faster or farther dispersing populations increase with time. However, Figs. 1b, 2c, 3b, 4b, 5b, and 6b show that ρ_{r_2} and ρ_{p_2} are sometimes increasing and sometimes decreasing. In fact, not surprisingly, the oscillations in the proportions have the same frequency as the oscillations of the density waves in space. Hence, we want to show that ρ_{r_2} and ρ_{p_2} always increase over one period of a wave even though there is some decrease during part of that period.

The oscillations in the proportions arise for the following reason. (We consider diffusion of the prey populations. A similar argument applies to the predator populations and for dispersal probability and distance.) Where the prey densities are at their maximal value diffusion will lower the prey densities at that point. Conversely, where the prey densities are at their minimal value diffusion will increase the prey density at that point. In other words, prey flow from high density to low density regions in space. Moreover, the faster the diffusion the greater the flow. Hence, where the prey densities are high (in fact, when $\nabla^2 r < 0$) proportionately less of the slower diffusing prey leaves these points in space than the faster diffusion prey and, therefore, the proportion of the slower diffusing prey at that point increases more than the proportion of the faster diffusing prey. Conversely, at low prey densities (when $\nabla^2 r > 0$) proportionately more faster diffusing prey enter a point in space and the proportion of these prey increases more than the proportion of the slower diffusing prey. Hence, at a given position in space, when the prey density is high the proportion of slower diffusing prey increases and when the prey density is low the proportion of the faster diffusing prey increases. Therefore we see oscillations in the proportions of the prey at the same frequency as the oscillations of the density waves.

What we have not explained is why, for the faster diffusing prey, there is more increase in its proportion than decrease over one period at a given point in space. The theory developed next tackles this problem. We first derive a theory for continuous time systems and compare the predictions to the 1D and 2D PDE predator–prey models and the 2D IO predator–prey model. Then we derive a theory for discrete time systems and compare the predictions to the 1D and 2D CML host–parasitoid models and the 2D IO host–parasitoid model.

3.3. Continuous Time

Consider two prey populations, $r_i = r_i(\mathbf{x}, t)$, and two predator populations, $p_i = p_i(\mathbf{x}, t)$, where t and $\mathbf{x}$ represent time and space. Let

$$r(\mathbf{x}, t) = r_1(\mathbf{x}, t) + r_2(\mathbf{x}, t) \tag{11}$$

$$p(\mathbf{x}, t) = p_1(\mathbf{x}, t) + p_2(\mathbf{x}, t) \tag{12}$$

for notational convenience. The prey and predator populations interact with the following dynamics,

$$\dot{r}_i = f(r, p)\, r_i + d_{r_i} \nabla^2 r_i \tag{13}$$

$$\dot{p}_i = g(r, p)\, p_i + d_{p_i} \nabla^2 p_i \tag{14}$$

(cf., Eqs. (1) and (2)), where f and g are chosen so that the system exhibits oscillations and d_{r_i} and d_{p_i} are the diffusion coefficients of the prey and the predator populations, respectively. We will consider the competition between the prey populations; similar results can be derived for the predators. Individuals in the two populations are identical except that r_2 has a higher diffusion coefficient than r_1:

$$d_{r_1} < d_{r_2}. \tag{15}$$

The fraction of prey r_i is given by

$$\rho_{r_i} = \frac{r_i}{r}. \tag{16}$$

The criterion for r_2 to exclude r_1 is

$$\rho_{r_2}(\mathbf{x}, t+T) - \rho_{r_2}(\mathbf{x}, t) > 0 \tag{17}$$

over all periods (Figs. 1b, 2c, and 5b), where T is the wave period. The LHS can be rewritten as

$$\int_t^{t+T} \dot{\rho}_{r_2}(\mathbf{x}, t)\, dt. \tag{18}$$

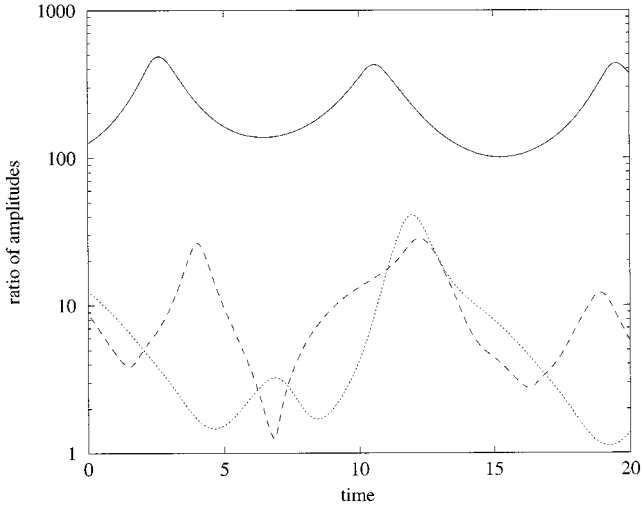

FIG. 8. The ratio of the magnitude of the third term and the first two terms in Eq. (21) as given by Eq. (65) over 20 time units in the 1D PDE simulation (solid line) and in the 2D PDE simulation within a spiral core (dotted line) and within a spiral arm (dashed line). The ratio is always greater than 1 and often much larger, allowing the assumption that the first two terms can be neglected.

Differentiating ρ_{r_2} with respect to time gives

$$\dot{\rho}_{r_2} = \frac{r_1 \dot{r}_2 - r_2 \dot{r}_1}{r^2}. \tag{19}$$

Substituting in Eq. (13) gives

$$\dot{\rho}_{r_2} = \frac{r_1 d_{r_2} \nabla^2 r_2 - r_2 d_{r_1} \nabla^2 r_1}{r^2}. \tag{20}$$

Note that ρ_{r_2} does not depend explicitly on the f and g reaction terms in Eqs. (13) and (14) but only implicitly through r_1 and r_2, which are oscillatory solutions of these equations.

Unfortunately we cannot proceed further without making a simplifying assumption. The second derivative of r_i with respect to space is given by

$$\nabla^2 r_i = r\, \nabla^2 \rho_{r_i} + 2\, \nabla r \cdot \nabla \rho_{r_i} + \rho_{r_i} \nabla^2 r. \tag{21}$$

In Appendix B and Fig. 8 we show that the amplitude of the third term is 100–1000 times larger in the 1D simulation and 1–50 times larger in the 2D simulation than the amplitude of the sum of the first two terms. Therefore, we assume that the first two terms are negligible. In fact, assuming this is equivalent to assuming that

$$\rho_{r_i}(\mathbf{x}, t) = \rho_{r_i}(t), \tag{22}$$

i.e., ρ_{r_i} is constant over all space. This is not true, hence we cannot now find an exact solution to the problem. However, an approximate analytical solution is still tractable.

Substituting Eqs. (16) and (22) into Eq. (20) gives

$$\dot{\rho}_{r_2} = \frac{\rho_{r_1}\, \rho_{r_2}(d_{r_2} - d_{r_1})\, \nabla^2 r}{r}. \tag{23}$$

Every term except the second derivative of r is positive. As r is oscillatory $\nabla^2 r < 0$ when r takes on high values and $\nabla^2 r > 0$ when r takes on low values. This means that if r is high for roughly the same length of time that it is low then Eq. (18) is greater than 0, implying that ρ_{r_2} always increases over one period. This can be seen intuitively by sketching $\nabla^2 r/r$ over one period. Because we are considering an arbitrary period of a wave, r_2 will exclude r_1.

To determine how fast r_2 excludes r_1 an exact form for r must be assumed. In general, a closed analytical form cannot be found for reaction–diffusion equations such as Eqs. (13) and (14). Thus, we choose a form for r that captures the local spatial behaviour of the oscillatory dynamics of Eqs. (13) and (14), realising that this further approximation to the real system could cause further divergence between it and our derived approximation. We take the simplest form for r in one dimension,

$$r(x, t) = \bar{r} + A_r \cos(kx - \omega t), \tag{24}$$

where $\bar{r}$ is the mean value of r, A_r the amplitude of the oscillations, k the wavenumber, and ω the temporal frequency. By this equation we do not mean to imply that the whole of space is covered by plane waves, but just that the local behaviour at a given point in space can be approximated by this form.

The second derivative of r with respect to x is

$$\frac{\partial^2 r}{\partial x^2} = -k^2(r - \bar{r}). \tag{25}$$

Substituting Eq. (25) into Eq. (23) and using the fact that $\rho_{r_1} = 1 - \rho_{r_2}$ gives

$$\dot{\rho}_{r_2} = -\rho_{r_2}(1 - \rho_{r_2})\, k^2(d_{r_2} - d_{r_1}) \cdot \frac{r - \bar{r}}{r}. \tag{26}$$

This can be integrated,

$$\int_{\rho_{r_2}(0)}^{\rho_{r_2}(t)} \frac{1}{\rho_{r_2}(1 - \rho_{r_2})}\, d\rho_{r_2} = -k^2(d_{r_2} - d_{r_1}) \int_0^t \frac{A_r \cos(kx - \omega t)}{\bar{r} + A_r \cos(kx - \omega t)}\, dt, \tag{27}$$

where $\rho_{r_2}(0)$ is the value of ρ_{r_2} at $t = 0$. The integral on the RHS is possible but rather messy. However, we can use the fact that the integrand is oscillatory with period $T = 2\pi/\omega$ at a fixed position x. Therefore, we make a change of variables so that $t = nT$, where n is the number of whole periods the integral is taken over. Thus, Eq. (27) becomes

$$\ln\left(\frac{\rho_{r_2}(nT)(1 - \rho_{r_2}(0))}{\rho_{r_2}(0)(1 - \rho_{r_2}(nT))}\right) = -k^2(d_{r_2} - d_{r_1})\, n \int_{-\pi}^{\pi} \frac{A_r \cos\theta}{\bar{r} + A_r \cos\theta}\, d\theta \tag{28}$$

$$= \lambda_r nT, \tag{29}$$

where

$$\lambda_r = k^2(d_{r_2} - d_{r_1})\left(\frac{\bar{r}}{\sqrt{\bar{r}^2 - A_r^2}} - 1\right). \tag{30}$$

Rearranging Eq. (29) gives

$$\rho_{r_2}(nT) = \frac{\rho_{r_2}(0)\, e^{\lambda_r nT}}{1 - \rho_{r_2}(0) + \rho_{r_2}(0)\, e^{\lambda_r nT}}, \tag{31}$$

which describes a sigmoid shaped curve that tends to 1 (0) as t tends to ∞ ($-\infty$), respectively.

3.3.1. *Comparison to Simulations.* We now wish to see if the approximate analytical solution can describe the results of the simulations. The derivation of the theory has assumed that the proportions do not change over space and that the oscillations are pure sine waves. A sine wave has a well defined mean and amplitude. This is rarely the case in nonlinear models such as Eqs. (1), (2), (7), and (8). Figure 2b shows a typical example of the modulations in the amplitudes. Another problem is the increase in the size of the patterns as the slower diffusing population is excluded. We have assumed a fixed wavelength in Eq. (24). All this leads to the conclusion that the predictions of the theory will only be rough approximations to the simulations.

The wavelength can be approximated either by eye or by calculating ω and v, the wave speed ($k = \omega/v$). ω can be calculated, for example, by performing a Fourier transform on a time series of the population density at a given point in space. v is calculated by dividing the distance traveled by a wave in a given amount of time. The best method we have found for calculating $\bar{r}$ and $\bar{p}$ is to calculate the mean value of time series $r(\mathbf{x}, t)$ and $p(\mathbf{x}, t)$ respectively. The best method we have found for

calculating A_r and A_p for continuous state systems is to calculate the averages of the minimum values of each wave and subtract these values from $\bar{r}$ and $\bar{p}$ respectively. The mean of the minimums is used because this always gives $A_r < \bar{r}$ ($A_r > \bar{r}$ implies negative densities). The mean of the maximums can, and often does give $A_r > \bar{r}$. For discrete state systems a problem arises because the minimum of a wave is normally zero because of local extinction of the population. This gives $A_r = \bar{r}$, which is not true. Several methods were tried using the maximums for the calculation of the means but problems arise because the waves are not nicely behaved sine waves; the maximums tend to be very large compared with the mean. The best method we have found so far is to calculate the standard deviation of the time series. However, the standard deviation can be greater than the mean. So to use the standard deviation as a measure of the amplitude of the waves we halve its value.

The choice of an approximation method is somewhat arbitrary and depends on the data set available. We have data that span many generations and can, therefore, take time averaged measures. Other data sets may contain only a few generations. However, experimenting suggests that even very rough approximations can still give correct order of magnitude predictions. Table 1 lists the values for $\bar{r}$, A_r, λ_r, $\bar{p}$, A_p, λ_p, and k for all the simulations in the second section.

Figure 9 shows the comparison of the theory (Eq. (31)) to the continuous time simulations ((a) 1D PDE predator–prey, (b) 2D PDE predator–prey, (c) 2D IO predator–prey). As expected there is some difference because of the assumptions made in the theory and the rough approximations of $\bar{r}$, $\bar{p}$, A_r, A_p, and k. Notwithstanding this, the approximate analytical solution does give the right order of magnitude for the exclusion time. The worst case is that for the continuous time IO model, which is approximately a factor of 2 out. It is difficult to say which of the assumptions we have made contribute most to the observed discrepancies between simulation and theory. This is because relaxing any of the assumptions to observe its effect would mean that an analytical analysis would become intractable.

3.3.2. *Neutral Competition.* Locally competition is always neutral because we have defined per capita growth rates as being identical for both populations (f and g in Eqs. (13) and (14)). Dispersal introduces non-local competition by inducing spatial pattern formation. However, non-local neutral competition occurs when $\lambda_r = 0$, i.e., r_2 can neither invade nor exclude r_1. $\lambda_r = 0$ can occur in two circumstances; when $A_r = 0$, i.e., when there are no oscillations, and when $k = 0$, i.e., when there are no waves, the spatially homogeneous case.

The first case typically occurs in spiral cores where the amplitude of the oscillations approach zero. In none of the PDE simulations in this paper, however, are there stable spiral cores (or more appropriately defects in one dimension) and, hence, positions in space where $A_r = 0$. They may exist for a long period of time but in the end they are annihilated. Thus, r_2 can invade at all positions

TABLE 1

The Approximated Values of $\bar{r}$, A_r, $\bar{p}$, A_p, and k and the the Calculated λ_r and λ_p Values for the Six Simulations Described in the Simulations Section and the Dispersal Probability Simulation (Last Column)

	1D PDE predator–prey	2D PDE predator–prey	1D CML host–parasitoid	2D CML host–parasitoid	2D IO predator–prey	2D IO host–parasitoid	1D CML host–parasitoid
$\bar{r}$	0.268	0.221	32.6	27.8	2.26	2.86	34.7
A_r	0.266	0.196	28.2	17.3	1.89	2.27	30.8
$\bar{p}$	2.25	2.4	11.9	10.115	13.2	2.51	
A_p	1.25	0.9	11.0	10.107	6.66	1.89	
k	0.031	0.22	0.24	0.57	0.29	0.52	0.25
λ_r	0.0039	0.029	1.24	1.25	0.069	1.51	1.06
λ_p	0.0001	0.0019	1.41	3.96	0.013	1.44	
d_{r_1}	0.5	0.5	2	1	2	2	2
d_{r_2}	1	1	3	2	3	3	2
d_{p_1}	0.5	0.5	2	1	2	2	2
d_{p_2}	1	1	3	2	3	3	
α_{r_1}			0.2	0.2	1	1	0.2
α_{r_2}			0.2	0.2	1	1	0.4
α_{p_1}			0.9	0.9	1	1	0.9
α_{p_1}			0.9	0.9	1	1	

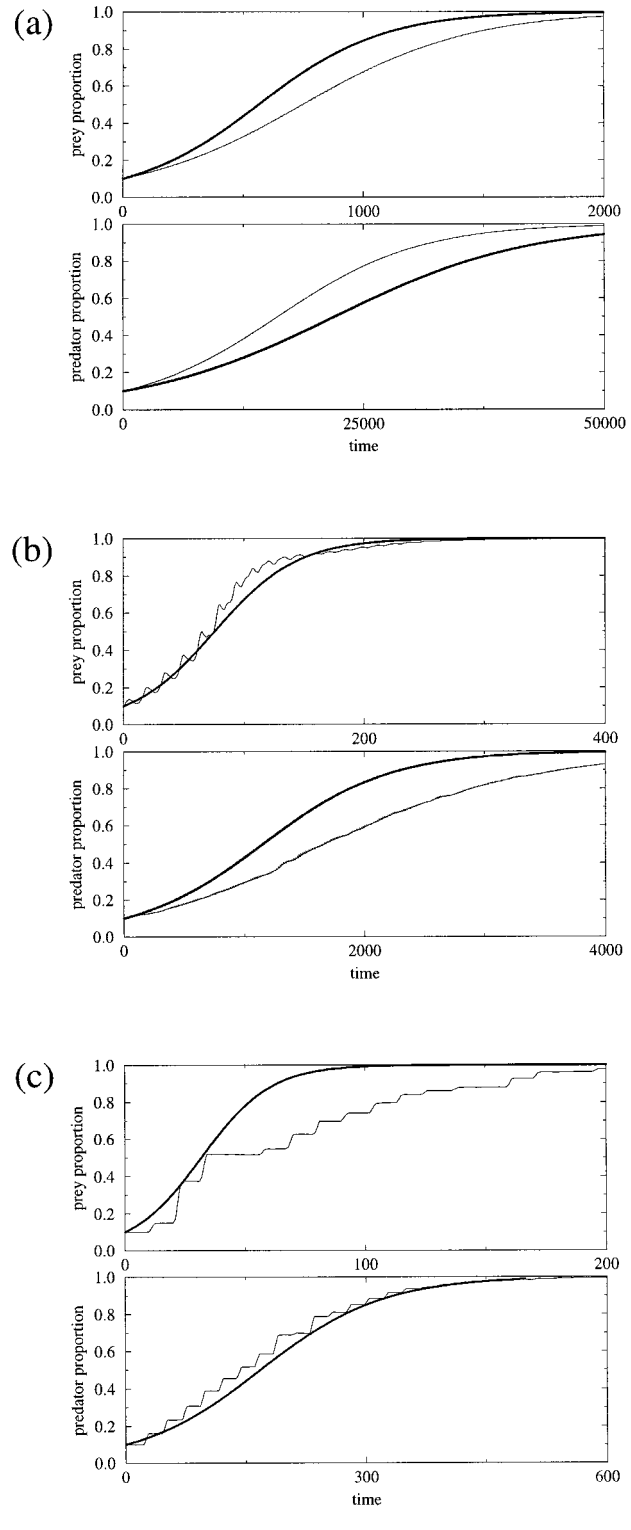

FIG. 9. Comparison of simulation and theory (Eq. (31)) for continuous time systems. We plot ρ_{r_2} and ρ_{p_2} (thin lines simulation, thick lines theory). (a) 1D PDE predator–prey simulation of Fig. 1. (b) 2D PDE predator–prey simulation of Fig. 2. (c) 2D IO predator–prey simulation of Fig. 5.

in space given enough time. The second case is intuitively obvious: If there are no waves it makes no difference at what rate an organism diffuses; all organisms see exactly the same environment and hence there is no competitive pressure. This case could arise if the spatial domain was very small, on the order of the diffusion coefficient.

3.3.3. *Cost of Dispersal.* So far we have assumed that the two competing populations are identical in every respect except their rates of diffusion. What happens if this is not the case? A good example is if there is a cost to having a higher diffusion rate such that it incurs a lower growth rate. For example, for the prey, this might mean that $a_1 > a_2$, i.e., the net growth rate of the slower diffusing prey population is larger than that of the faster diffusing prey population because it has, for example, more time or energy for the raising of its offspring. Substituting $a = a_1, a_2$ into Eq. (13) and following the arguments for the derivation of λ_r from Eq. (20) to (30) gives

$$\lambda_{r_{\text{cost}}} = \lambda_r - (a_1 - a_2), \tag{32}$$

where λ_r is defined in Eq. (30). Figure 10 shows simulations of the 1D PDE predator–prey for different values of $\Delta_a = a_1 - a_2$. When $\Delta_a > \lambda_r$, $\lambda_{r_{\text{cost}}}$ is negative and hence the cost of dispersal outweighs the benefits gained and,

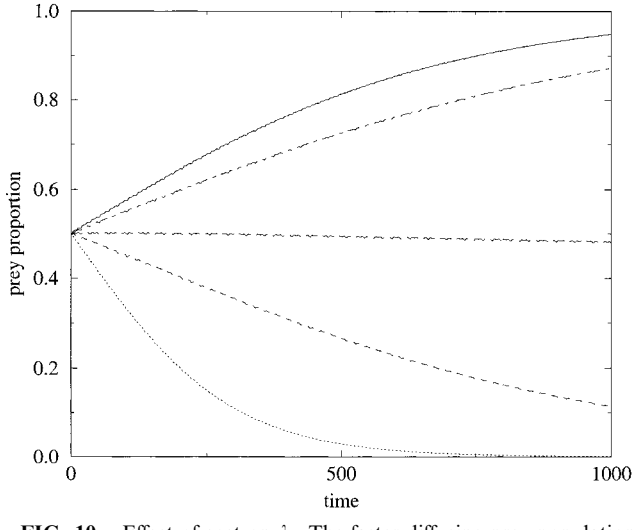

FIG. 10. Effect of cost on λ_r. The faster diffusing prey population has a smaller growth rate. The effect of which on λ_r is given by Eq. (32). The simulation is the 1D PDE predator–prey, all parameters and boundary conditions as in Fig. 1. The initial prey densities are $r_1 = r_2$. The parameter a_2 is kept constant; a_1 is varied. Let $\Delta_a = a_1 - a_2$. Solid line $\Delta_a = 0$, dot–dashed line $\Delta_a = 0.001$, long dashed line $\Delta_a = 0.003$, short dashed line $\Delta_a = 0.005$, dotted line $\Delta_a = 0.01$. From the theory we predicted $\lambda_r = 0.0039$ (Table 1) but from these simulations it appears that it should be closer to 0.003, which is a 0.14% difference in the growth rates of the prey.

therefore, the slower diffusing population excludes the faster. On the other hand, when $\Delta_a < \lambda_r$, the cost is not so prohibitive, nevertheless it does increase the exclusion time of the slower diffusing population. Δ_a can be adjusted so that it exactly counterbalances the benefit of dispersal. This is seen as the continued coexistence of both populations for very long time periods and occurs when $\Delta_a = 0.003$ in Fig. 10. This means that the value of $\lambda_r = 0.0039$ calculated earlier was too high by about 9×10^{-4}. The above argument holds for any of the parameters in Eqs. (1) and (2). If all parameters are different then $\lambda_{r_{\text{cost}}} = \lambda_r - (a_1 - a_2) - \bar{r}(b_1 - b_2)$ and $\lambda_{p_{\text{cost}}} = \lambda_p - (c_1 - c_2)$.

3.4. Discrete Time

The discrete time case is very similar to the continuous case. However, now we consider maximum dispersal distance as opposed to diffusion rate.

Consider two prey populations, $r_i = r_i(\mathbf{x}, t)$, and two predator populations, $p_i = p_i(\mathbf{x}, t)$, and let

$$r(\mathbf{x}, t) = r_1(\mathbf{x}, t) + r_2(\mathbf{x}, t) \tag{33}$$

$$p(\mathbf{x}, t) = p_1(\mathbf{x}, t) + p_2(\mathbf{x}, t) \tag{34}$$

for notational convenience. At the start of generation t there is dispersal of prey and predators,

$$r'_i(\mathbf{x}, t) = (1 - \alpha_r)\, r_i(\mathbf{x}, t) + \alpha_r \int_{-\infty}^{\infty} r_i(\mathbf{x} - \xi, t)\, D_{r_i}(\xi)\, d\xi \tag{35}$$

$$p'_i(\mathbf{x}, t) = (1 - \alpha_p)\, p_i(\mathbf{x}, t) + \alpha_p \int_{-\infty}^{\infty} p_i(\mathbf{x} - \xi, t)\, D_{p_i}(\xi)\, d\xi, \tag{36}$$

where α_r and α_p are the dispersal probabilities of prey and predators, respectively, and $D_{r_i}(\mathbf{x})$ and $D_{p_i}(\mathbf{x})$ are the prey and predator dispersal functions, respectively, and

$$\int_{-\infty}^{\infty} D_{r_i}(\mathbf{x})\, d\mathbf{x} = 1 \tag{37}$$

$$\int_{-\infty}^{\infty} D_{p_i}(\mathbf{x})\, d\mathbf{x} = 1. \tag{38}$$

For convenience we denote the convolution of the prey and predator densities with their dispersal functions as $r_i * D_{r_i}$ and $p_i * D_{p_i}$, respectively. Also let

$$r'(\mathbf{x}, t) = r'_1(\mathbf{x}, t) + r'_2(\mathbf{x}, t) \tag{39}$$

$$p'(\mathbf{x}, t) = p'_1(\mathbf{x}, t) + p'_2(\mathbf{x}, t) \tag{40}$$

for notational convenience.

The prey and predator densities in the next generation are given by

$$r_i(\mathbf{x}, t+1) = r'_i(\mathbf{x}, t) \cdot f(r'(\mathbf{x}, t), p'(\mathbf{x}, t)) \tag{41}$$

$$p_i(\mathbf{x}, t+1) = p'_i(\mathbf{x}, t) \cdot g(r'(\mathbf{x}, t), p'(\mathbf{x}, t)) \tag{42}$$

(cf. Eqs. (7) and (8)), where f and g are chosen so that the system exhibits oscillations. We will consider the competition between the two prey populations. Similar results can be derived for the predators. Individuals in the two populations are identical except that r_2 disperses farther than r_1 on average. In terms of the dispersal functions this means

$$\text{Variance}(D_{r_1}(\mathbf{x})) < \text{Variance}(D_{r_2}(\mathbf{x})). \tag{43}$$

The fraction of prey r_i is given by

$$\rho_{r_i} = \frac{r_i}{r}. \tag{44}$$

The criterion for r_2 to exclude r_1 is

$$\rho_{r_2}(\mathbf{x}, t+T) - \rho_{r_2}(\mathbf{x}, t) > 0 \tag{45}$$

over all periods (Figs. 3b, 4b, and 6b), where T is the wave period. The LHS can be rewritten as

$$\sum_{t}^{t+T-1} \rho_{r_2}(\mathbf{x}, t+1) - \rho_{r_2}(\mathbf{x}, t). \tag{46}$$

Let

$$\phi_{r_2}(\mathbf{x}, t+1) = \rho_{r_2}(\mathbf{x}, t+1) - \rho_{r_2}(\mathbf{x}, t). \tag{47}$$

Using Eq. (44) and substituting in (41) we get

$$\rho_{r_2}(\mathbf{x}, t+1) = \frac{r_2(\mathbf{x}, t+1)}{r(\mathbf{x}, t+1)} = \frac{r'_2(\mathbf{x}, t)}{r'(\mathbf{x}, t)}. \tag{48}$$

Substituting this into Eq. (47) and using Eqs. (33), (39), and (44) gives

$$\phi_{r_2} = \frac{r_1 r'_2 - r_2 r'_1}{r r'}. \tag{49}$$

Again, to proceed further, we use the assumption

$$\rho_{r_i}(\mathbf{x}, t) = \rho_{r_i}(t), \tag{50}$$

which gives $r'_i = \rho_{r_i} r * D_{r_i}$. Substituting this into Eq. (49) and using the convolution notation we get

$$\phi_{r_2} = \frac{\rho_{r_1}\rho_{r_2} r * (D_{r_2} - D_{r_1})}{r'}. \tag{51}$$

Every term except the convolution of r is positive. As r is oscillatory $r * (D_{r_2} - D_{r_1}) < 0$ when r takes on high values and $r * (D_{r_2} - D_{r_1}) > 0$ when r takes on low values. This means that if r is high for roughly the same length of time that it is low then Eq. (46) is greater than 0, implying that ρ_{r_2} always increases over one period. And because we are considering an arbitrary period, r_2 will exclude r_1.

Again, taking a specific function for r in one space dimension to determine how fast exclusion occurs,

$$r(x, t) = \bar{r} + A_r \cos(kx - \omega t). \tag{52}$$

We use the simplest form for D_{r_i},

$$D_{r_i}(x) = \begin{cases} \dfrac{1}{2d_{r_i}} & \text{if} \quad -d_{r_i} \leqslant x \leqslant d_{r_i} \\ 0 & \text{otherwise,} \end{cases} \tag{53}$$

where

$$d_{r_1} < d_{r_2}. \tag{54}$$

This gives

$$r * D_{r_i} = \bar{r} + (r - \bar{r}) \frac{\sin(kd_{r_i})}{kd_{r_i}} \tag{55}$$

$$= \bar{r} + (r - \bar{r}) \left(1 - \frac{k^2 d_{r_i}^2}{6}\right), \tag{56}$$

assuming kd_{r_i} is small. (The values for k given in Table 1 show that $kd_{r_i} < 1$ which is good enough considering the other assumptions we have made.) Substituting Eq. (56) into Eq. (51) and using $\rho_{r_1} = 1 - \rho_{r_2}$:

$$\phi_{r_2} = \frac{\rho_{r_2}(1 - \rho_{r_2})(r - \bar{r})\, k^2 (d_{r_2}^2 - d_{r_1}^2)}{-6r + (r - \bar{r})\, k^2 d_{r_1}^2 + \rho_{r_2}(r - \bar{r})\, k^2 (d_{r_2}^2 - d_{r_1}^2)}. \tag{57}$$

Using Eq. (47) gives

$$\rho_{r_2}(x, t+1) = \frac{6r - (r - \bar{r})\, k^2 d_{r_2}^2}{6r - (r - \bar{r})\, k^2 d_{r_1}^2 - (r - \bar{r})\, k^2 (d_{r_2}^2 - d_{r_1}^2)\ \rho_{r_2}(x, t)} \times \rho_{r_2}(x, t), \tag{58}$$

which describes a sigmoid shaped curve that tends to 1 (0) as t tends to ∞ ($-\infty$), respectively.

The nonlinearities in Eq. (58) mean there is no simple method of determining an analytical solution for it. So far we have not been able to find one, if one exists at all. However, we can get a rough estimate of the rate of exclusion by linearising Eq. (58) when ρ_{r_2} is small,

$$\rho_{r_2}(x, t+1) = \lambda_r\ \rho_{r_2}(x, t), \tag{59}$$

where

$$\lambda_r = 1 + \frac{k^2 (r - \bar{r})(d_{r_2}^2 - d_{r_1}^2)}{k^2 (r - \bar{r})\, d_{r_1}^2 - 6r}. \tag{60}$$

Equation (60) is still a function of r and hence, of t. To remove this dependence we must choose a fixed value for r. As a first approximation we choose a value for r when ρ_{r_2} is increasing fastest. This occurs when r is at its minimum value, i.e., when $r = \bar{r} - A_r$. Substituting this into Eq. (60) we get

$$\lambda_r = 1 + \frac{A_r k^2 (d_{r_2}^2 - d_{r_1}^2)}{6(\bar{r} - A_r) + A_r k^2 d_{r_1}^2}. \tag{61}$$

Hence, we expect the rate of exclusion to increase with increasing amplitude, increasing difference in maximum dispersal distances, and decreasing wavelength, all the same as for the continuous case. The equation also predicts faster exclusion in shocks than in defects (cores).

3.4.1. *Comparison to Simulations.* We now wish to see if the approximate analytical solution can describe the results of the simulations. We use the same techniques as mentioned for the continuous time systems to approximate the parameters in Eqs. (58) and (61). Their values are given in Table 1. Figure 11 shows the comparison of the discrete time simulations to the solution (58) which shows reasonable agreement even with the rough approximations ((a) 1D CML host–parasitoid, (b) 2D CML host–parasitoid, (c) 2D IO host–parasitoid).

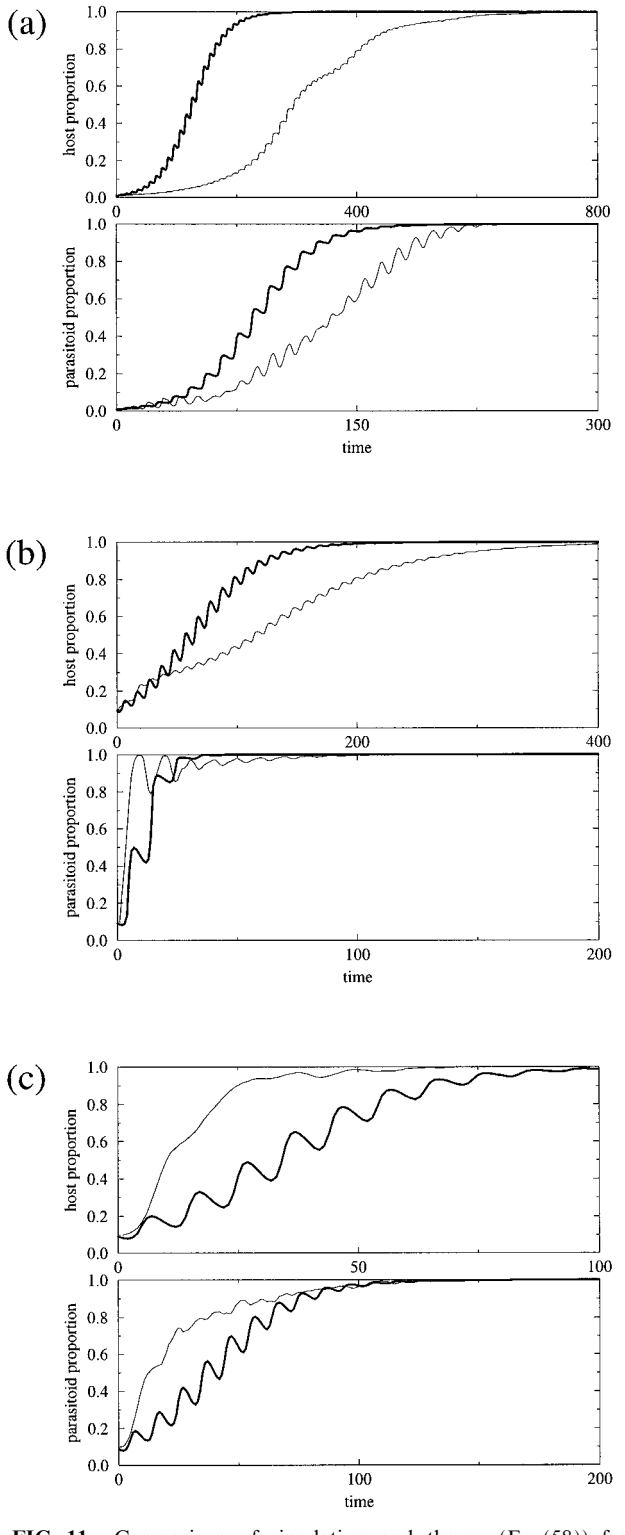

FIG. 11. Comparison of simulation and theory (Eq. (58)) for discrete time systems. We plot ρ_{r_2} and ρ_{p_2} (thin lines simulation, thick lines theory). (a) 1D CML host–parasitoid simulation of Fig. 2. (b) 2D CML host–parasitoid simulation of Fig. 4. (c) 2D IO host–parasitoid simulation of Fig. 6.

3.4.2. *Dispersal Probability.* We have only considered the case where competing organisms have the same dispersal probability and the only difference between the organisms is the maximum distance they disperse. Now we consider the case where the maximum dispersal distances are the same but the probabilities of dispersal are different, i.e., $D_{r_1} = D_{r_2} = D_r$, implying that $d_{r_1} = d_{r_2} = d_r$. Then the prey post–dispersal densities are given by

$$r_i'(\mathbf{x}, t) = (1 - \alpha_{r_i})\, r_i(\mathbf{x}, t) + \alpha_{r_i} \int_{-\infty}^{\infty} r_i(\mathbf{x} + \xi, t)\, D_r(\xi)\, d\xi. \tag{62}$$

Using this equation and following the same arguments from Eq. (51) to Eq. (61) we get for λ_r

$$\lambda_r = 1 + \frac{A_r k^2 d_r^2 (\alpha_{r_2} - \alpha_{r_1})}{6(\bar{r} - A_r) + A_r k^2 d_r^2 \alpha_{r_1}}. \tag{63}$$

Therefore, competition favours prey that are more likely to disperse. Figure 12 shows the proportion of r_2 and the predicted proportion for the 1D CML host–parasitoid model with $d_r = 2$ and $\alpha_{r_1} = 0.2$ and $\alpha_{r_2} = 0.4$ (the means and amplitudes are given in the last column of Table 1). Note that λ_r depends linearly on the dispersal probabilities but quadratically on the maximum dispersal distance. This suggests, and intuitively it seems correct, that the dispersal probability is the discrete time analogue of continuous time diffusion as λ_r depends linearly on the diffusion coefficients.

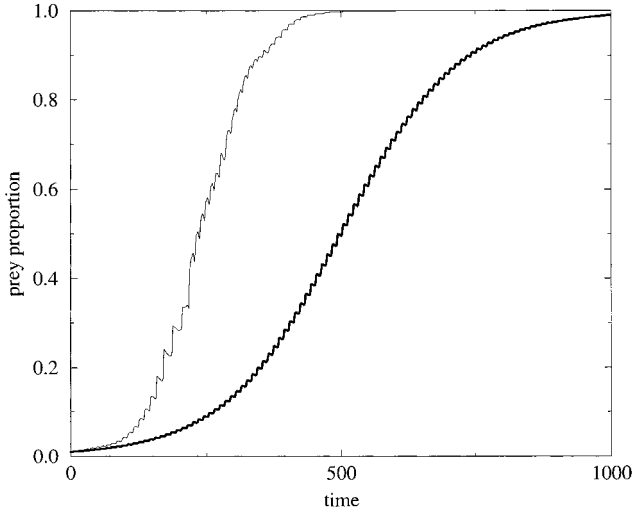

FIG. 12. Comparison of simulation and theory (Eq. (63)) for different prey dispersal probabilities in the 1D CML host–parasitoid model. All parameters, initial conditions, and boundary conditions are the same as in Fig. 3, except $d_{r_1} = d_{r_2} = d_r = 2$ and $\alpha_{r_1} = 0.2$ and $\alpha_{r_2} = 0.4$. We plot ρ_{r_2} (thin lines simulation, thick lines theory).

3.4.3. *Coexistence.* Comins and Hassell (1996) have shown that a parasitoid population with a certain dispersal rate and a certain birth (or attack) rate can either exclude, coexist with, or be excluded by a parasitoid population with a lower dispersal rate and a higher birth (or attack) rate. The outcome depends strongly on the relative difference between the two populations' birth (or attack) rates. If coexistence occurs the weaker dispersing population only occupies the spiral cores.

We have repeated some of the work by Comins and Hassell (1996) and calculated the exclusion rates to see if we could explain their results. Their system is a one-host–two-parasitoid model with $d_r = 1$ and $d_{p_i} = d_p = 1$. They use a slightly different notation with $\mu_N = \alpha_r$ and $\mu_{P_i} = \alpha_{p_i}$. The ratio of the birth (attack) rates of the weak dispersing population to the strong dispersing population is α; we will use β. If $\beta = 1$ the two parasitoid populations are effectively identical except for their dispersal rates. We will only look at three cases for brevity. We take $\alpha_r = 0.5$, $\alpha_{p_1} = 0.5$, and $\alpha_{p_2} = 0.05$ (i.e., p_2 is the weaker dispersing population) and values of 1, 1.3, and 2 for β that correspond with p_2 excluded by, coexisting with, and excluding p_1, respectively (see their Figs. 3a, 5). We ran the simulations for 100 generations and calculated $\bar{p}$, A_p, and λ_p in a defect of a spiral core and the spiral arm. The exclusion rate λ_p in our notation is given by

$$\lambda_p = \beta\left(1 + \frac{A_p k^2 d_p^2(\alpha_{p_2} - \alpha_{p_1})}{6(\bar{p} - A_p) + A_p k^2 d_p^2 \alpha_{p_1})}\right) \qquad (64)$$

The results of the three simulations are given in Table 2.

For $\beta = 1$, $\lambda_p < 1$ in the arm and the defect and hence p_2 is excluded everywhere by p_1. For $\beta = 1.3$, $\lambda_p > 1$ in the defect but < 1 in the arm, i.e., p_2 excludes p_1 in the defect but not in the arm. At first sight this would seem to agree with the coexistence reported by Comins and Hassell (1996), but if one considers a property of spiral cores in ecological systems this is not so obvious. It has been shown that spiral cores act as the source of all genetic information in a spiral (Boerlijst and Hogeweg, 1991a; Boerlijst and Hogeweg, 1991b; Savill *et al.*, 1997), i.e., all individuals in a spiral are descended from individuals that once existed in the core. If this is so p_2 excluding p_1 in the core would mean it excluded p_1 in the whole spiral. The reason this does not occur is shown in Fig. 13. p_2 only excludes p_1 near the defect, further away but still in the core, p_1 excludes p_2. Therefore, they can coexist in the core but p_2 is excluded in the arm. For $\beta = 2$, p_2 excludes p_1 in the whole core and hence in the whole spiral even though $\lambda_p < 1$ in the arm.

TABLE 2

The Approximated Values of $\bar{p}$, A_p, and λ_p for the Simulations of the One-Host–Two-Parasitoid Models of Comins and Hassell (1996)

	β					
	1		1.3		2	
	defect	arm	defect	arm	defect	arm
$\bar{p}$	0.77	1.0261	0.75	1.0208	0.549	1.15776
A_p	0.28	1.0215	0.50	1.0170	0.51	0.15765
λ_p	0.99	0.26	1.25	0.31	1.57	0.25

Note. The values are calculated in a spiral defect and a spiral arm averaged over 100 generations for the different values of β (the relative fitness of p_2 over p_1); $k = 0.5$. The less likely dispersing population, p_2, is excluded by, coexists with, and excludes the stronger dispersing population p_1 for $\beta = 1$, 1.3, and 2, respectively. Other parameters and their corresponding names in their paper are $d_r = 1$, $d_{p_i} = d_p = 1$, $\mu_N = \alpha_r = 0.5$, $\mu_{P_1} = \alpha_{p_1} = 0.5$, $\mu_{P_2} = \alpha_{p_2} = 0.05$, and $\alpha = \beta$.

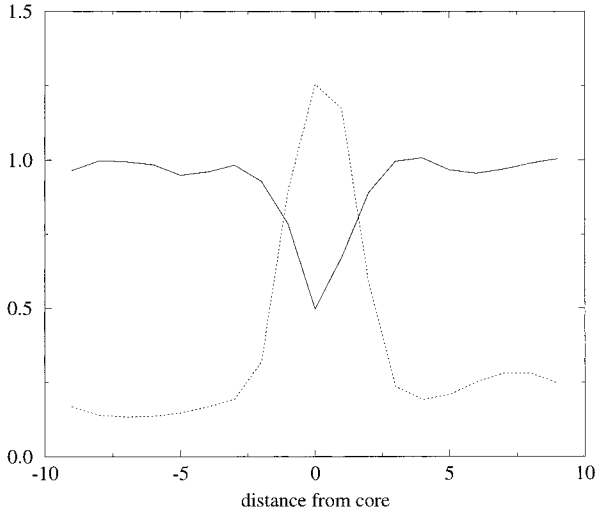

FIG. 13. The amplitude (A_p, solid line) and the competition rate (λ_p, dotted line) in a cross section through a spiral wave for $\beta = 1.3$ from Comins and Hassell (1996). The weaker dispersing population, p_2, can only exclude the stronger dispersing population, p_1, near the defect ($\lambda_p > 1$), but p_1 can exclude p_2 further from the defect but still in the core, and hence they coexist within the core. In the arm p_1 can exclude p_2 ($\lambda_p < 1$).

4. DISCUSSION AND CONCLUSION

Spatial oscillatory systems, whether continuous or discrete in time, space, or state, all exhibit the generic patterns of spiral waves and turbulence (Cross and Hohenberg, 1993). Sherratt *et al.* (1997) have also shown that turbulence arises in the wake of predator–prey invasion waves in a variety of oscillatory systems. We have shown that the effect of these generic patterns on the

competition between populations with different dispersal strategies is similar for both discrete and continuous systems. Moreover, we have also shown that the precise interactions between predators and prey do not affect the competitive behaviour. All that matters is that waves exist. This is not to say that the effect of the patterns on other processes in ecological systems, perhaps, for example, on foraging strategies, will be similar.

Previous models of the evolution of dispersal strategies have assumed that spatial and temporal patterns (variation) that can affect the fitness of the dispersing organisms are externally driven, e.g., by carrying capacity of a patch or random patch extinction. It is possible, however, that spatio-temporal patterns are due to self-structuring processes of the organisms themselves. In fact there will probably be a bit of both. The task of theoretical models is then to examine the relative strengths of externally and internally driven patterns, to find common ground, and to discover differences between them.

In this paper we have examined predator–prey population models that, because of their oscillatory dynamics, exhibit self-structuring into wave-like patterns in space. Competing populations have been assumed to be identical in every respect except for their dispersal strategy. This situation may arise in the case of a mutant invading a wildtype population. Both simulation results and mathematical theory predict that organisms are more likely to disperse and disperse farther in these waves. This is in direct agreement with many of the previous models that predicted increased dispersal in externally driven temporally varying environments (e.g., Levin *et al*., 1984). Our results can be intuitively understood: By definition waves structure the spatial distribution of organisms into regions of high and low density. In high density regions competition is most fierce for the scarce resource, whatever that may be. Therefore, it pays to disperse into low density regions where competition is weaker.

Previous modelling of spatio-temporal oscillations and competition have determined the effect of competition on the spatio-temporal oscillations, e.g., the spread of genetically engineered organisms (Cruywagen *et al*., 1996) and the effect of noise (Vilar and Solé, 1998). In this paper we have turned the process around and looked at the effect of spatio-temporal oscillations on competition. Although there is considerable evidence of temporal oscillations in the field, only very recently have the causes and effects of spatio-temporal oscillations been studied. A large problem to overcome is actually proving that waves exist. Waves are easy to see and analyse in computer simulations because all the data one requires are at hand. However, field study data can be noisy, absent, or taken over too short a time scale or at the wrong spatial resolution. Moreover, the collection of data may interfere with the dynamics of the ecological system. Hence, one has to rely on statistics to "observe" the waves, and then the data may only be suggestive of waves. Some ecological systems that have been proposed as exhibiting waves are the Canadian Horseshoe hare (Ranta *et al*., 1997b; Ranta *et al*., 1997a), wood lemmings in Norway and Sweden (Fredga *et al*., 1993), red grouse in Scotland (Moss *et al*., 1999), voles in Finland and France (Ranta and Kaitala, 1997) and Northern Britain (Lambin *et al*., 1998). Roland and Taylor (1997) observed spatial patterns of parasitic flies over a 3-year period; they did not hypothesize travelling waves but there is a distinct possibility that they exist.

The theory predicts that exclusion will be faster in waves with smaller wavelengths, larger amplitudes, and smaller means. Exclusion is also faster when the relative differences between the diffusion coefficients or the dispersal distances are larger. Considering the assumptions we have made, the theory and the simulations agree reasonably well. Even very rough approximations of the wave's properties are good enough to give the correct order of magnitude for the rate of exclusion. If a cost for dispersal is introduced then it is possible, if the cost is high enough, for the weaker dispersing population to exclude the stronger dispersing population. The simulations show clearly that the size of the patterns increases as the diffusion coefficient or maximum dispersal distance increases.

In this paper the boundary conditions do not affect the competitive exclusion with the spatial patterns. However, there are cases where the boundary conditions are important. In 1D zero boundary conditions behave like stable defects and hence waves are seen to originate from them. In 2D it is possible to have a short dispersing population "trapped" on the boundary with a far dispersing population rotating within spirals that are almost on the same scale as the spatial domain. This scenario can arise if the dispersal distance is allowed to evolve (Savill and Hogeweg, 1998). Roland and Taylor (1997) have observed that insect parasitoids that disperse shorter distances than their competitors have higher parasitism rates at the edges of the forests they inhabit.

We have only considered competition; the next logical step is to examine how dispersal strategies would evolve (Savill and Hogeweg, 1998). The theory presented in this paper suggests that populations should evolve to ever higher dispersal rates and/or distances given no cost to dispersal. However, as the dispersal rates and/or distances increase the size of the patterns also increase. There may come a point where the size of the patterns are on the same scale as the size of the space. At this point the patterns can disappear, leading to extinction. A more

interesting possibility for an evolving population is the process of speciation and the coexistence of more than one species.

APPENDIX A

The 2D individual oriented predator–prey model is defined as follows. Space is made up of a square lattice of 150×150 patches with zero or no-flux boundary conditions (numerous simulations suggest no difference in the results for the different boundary conditions). The oscillations of the PDE system are due to the Holling type II functional response which is the effect of the predators having a handling time, i.e., some time being taken to catch, consume, and digest a prey. To achieve oscillations in the IO model we must explicitly model a handling time.

To model continuous time, individuals are picked at random to be updated. If a prey is chosen to be updated it can either disperse according to the prey dispersal function (probability of dispersal is 100%) or give birth to a pre-determined number of offspring (2) if the prey-carrying capacity of the patch it occupies has not been reached (10). There is a 50% chance of either behaviour happening. A predator, if chosen, can either disperse according to the predator dispersal function (probability of dispersal is 100%) or die (50% chance) or attack a prey if one is available in the patch it occupies and if it is not already handling a prey. The handling time is set to one update step. Once a predator has eaten its prey it gives birth to a pre-determined number of offspring (5) if the predator-carrying capacity of the patch it occupies has not been reached (50). There is a $33.\dot{3}\%$ chance of any of the three behaviours happening.

Using the above parameters as default, each parameter was varied, keeping all other parameters equal to their default values. Predator and prey dispersal rates varied from 1% to 100%. The number of predator and prey offspring varied from 5 to 10 and 2 to 5 respectively. The predator and prey carrying capacities varied from 30 to 55 and 5 to 20, respectively. The predator handling time varied from 1 to 2. The predator death probability varied from 0.5 to 0.9. Quantitative results can vary but qualitative wave-like patterns are very easy to produce. This leads us to speculate that the precise interactions between predators and prey are not a factor in the results of this paper.

The discrete time host–parasitoid system is modelled as follows. In each generation hosts and parasitoids disperse in a random direction and to a distance determined by their dispersal function (100% chance of dispersal). After dispersal some hosts are killed if the total number of hosts in a patch exceeds the pre-determined carrying capacity (5). Each parasitoid in a patch can infect only one host (100% chance of infection). If there are more parasitoids than hosts some parasitoids will not infect hosts. Once parasitism has occurred uninfected hosts give birth to a pre-determined number of offspring (3) and die. Infected hosts are killed by the offspring of the parasitoid that infected them and a pre-determined number of parasitoid offspring survive (3). All parasitoids from the previous generation die. The cycle begins anew. Using the above parameters as default, each parameter was varied keeping all other parameters equal to their default values. Host and parasitoid dispersal rates varied between 1% and 100%. The number of host and parasitoid offspring varied between 2 and 10. The host carrying capacity varied between 2 and 20.

Again the exact parameters are not important, as long as the system oscillates to produce host–parasitoid waves, the farther dispersing hosts and parasitoids exclude the shorter dispersing hosts and parasitoids, respectively.

APPENDIX B

We want to show that the first two terms in Eq. (22) are smaller than the third term so that we can neglect these terms. To simply calculate the ratio of these terms is uninformative because they will equal zero at some positions in space. A better method is to calculate their integrals of their absolute values over a region of space S, then take their ratio, i.e.,

$$R = \frac{\int_S |\rho_{r_i} \nabla^2 r| \, dS}{\int_S |r \nabla^2 \rho_{r_i} + 2 \nabla r \nabla \rho_{r_i}| \, dS}. \tag{65}$$

This gives a measure of the ratio of the magnitude of the terms.

Figure 8 shows the value of R calculated over 20 time units for the 1D PDE simulation (solid line), the 2D PDE simulation within a core (dotted line), and the 2D PDE simulation within a spiral arm (dashed line). In the 1D case the third term averaged over the whole wave, is at least two orders of magnitude larger than the sum of the first two terms. The 2D case is worse in both the core and the spiral arm with the ratio, at some times, only slightly greater than 1. However, averaged over time, the third term is roughly 10 times larger than the sum of the first two terms. Therefore, in the 1D case we can safely assume the first two terms are negligible compared with the last term. In the 2D case the assumption can still be made but with weaker justification.

ACKNOWLEDGMENTS

N. Savill was supported by the Priority Program Nonlinear Systems of the Netherlands Organization for Scientific Research. The Dynamics Systems Lab provided the computer facilities.

REFERENCES

Bascompte, J., and Solé, R. V. (1996), Habitat fragmentation and extinction thresholds in spatially explict models, *J. Anim. Ecol.* **65**, 465–473.

Boerlijst, M. C., and Hogeweg, P. (1991a), Self-structuring and selection: Spiral waves as a substrate for evolution, *in* "Artificial Life II" (C. G. Langton, Ed.), pp. 255–276, Addison–Wesley, Redwood City, CA.

Boerlijst, M. C., and Hogeweg, P. (1991b), Spiral wave structure in pre-biotic evolution: Hypercycles stable against parasites, *Physica D* **48**, 17–28.

Boerlijst, M. C., Lamers, M. E., and Hogeweg, P. (1993), Evolutionary consequences of spiral waves in a host–parasitoid system, *Proc. Roy. Soc. London Ser. B* **253**, 15–18.

Comins, H. N., and Hassell, M. P. (1996), Persistence of multispecies host–parasitoid interactions in spatially distributed models with local dispersal, *J. Theor. Biol.* **183**, 19–28.

Comins, H. N., Hassell, M. P., and May, R. M. (1992), The spatial dynamics of host–parasitoid systems, *J. Anim. Ecol.* **61**, 735–748.

Cross, M. C., and Hohenberg, P. C. (1993), Pattern formation outside of equilibrium, *Rev. Mod. Phys.* **65**, 851–1112.

Cruywagen, G. C., Kareiva, P., Lewis, M. A., and Murray, J. D. (1996), Competition in a spatially heterogeneous environment: Modelling the risk of spread of a genetically engineered population, *Theor. Popul. Biol.* **49**, 1–38.

Durrett, R., and Levin, S. (1994), The importance of being discrete (and spatial), *Theor. Popul. Biol.* **46**, 363–394.

Fredga, K., Fredriksson, R., Bondrup-Nielson, S., and Ims, R. A. (1993), Sex ratio, chromosomes and isozymes in natural populations of wood lemming (*Myopus schisticolor*), *in* "The Biology of Lemmings" (N. C. Stenseth and R. A. Ims, Eds.), pp. 465–491, Academic Press, London.

Gustafson, E. J., and Gardner, R. H. (1995), The effect of landscape hetergeneity on the probability of patch colonization, *Bull. Math. Biol.* **57**, 507–526.

Hamilton, W. D., and May, R. M. (1977), Dispersal in stable habitats, *Nature* **269**, 578–581.

Hassell, M. P., Comins, H. N., and May, R. M. (1991), Spatial structure and chaos in insect population dynamics, *Nature* **353**, 255–258.

Hogeweg, P. (1988), MIRROR beyond MIRROR, puddles of LIFE, *in* "Artificial Life" (C. G. Langton, Ed.), pp. 297–316, Addison–Wesley, Redwood City, CA.

Hogeweg, P. (1994), Multilevel evolution: Replicators and the evolution of diversity, *Physica D* **75**, 275–291.

Holmes, E. E., Lewis, M. A., Banks, J. E., and Veit, R. R. (1994), Partial differential equations in ecology: Spatial interactions and population dynamics, *Ecology* **75**, 17–29.

Johnson, M. L., and Gaines, M. S. (1990), Evolution of dispersal: Theoretical models and empircal tests using birds and mammals, *Annu. Rev. Ecol. Syst.* **21**, 449–480.

Johst, K., and Brandl, B. (1997), Evolution of dispersal: The importance of the temporal order of reproduction and dispersal, *Proc. Roy. Soc. London Ser. B* **264**, 23–30.

Lambin, X., Elston, D. A., Petty, S. J., and MacKinnon, J. L. (1998), Spatial asynchrony and periodic travelling waves in cyclic populations of field voles, *Proc. Roy. Soc. London Ser. B* **265**, 1491–1496.

Levin, S. A., Cohen, D., and Hastings, A. (1984), Dispersal in patchy environments, *Theor. Popul. Biol.* **26**, 165–191.

McCauley, E., Wilson, W. G., and de Roos, A. M. (1996), Dynamics of age-structured predator-prey populations in space: Asymmetrical effects of mobility in juvenile and adult predators, *OIKOS* **76**, 485–497.

McPeek, M. A., and Holt, R. D. (1992), The evolution of dispersal in spatially and temporally varying environments, *Am. Nat.* **140**, 1010–1027.

Moss, R., Elston, D. A., and Watson, A. (1999), Spatial asynchrony and demographic travelling waves during red grouse population cycles, submitted for publication.

Nicholson, A. J., and Bailey, V. A. (1935), The balance of animal populations, I, *Proc. Zool. Soc. London* **3**, 551–598.

Ranta, E., and Kaitala, V. (1997), Travelling waves in vole population dynamics, *Nature* **390**, 456.

Ranta, E., Kaitala, V., and Lindströ, J. (1997a), Dynamics of Canadian lynx populations in space and time, *Ecography* **20**, 454–460.

Ranta, E., Lindströ, J., Kaitala, V., Kokko, H., Lindén, H., and Elle, E. (1997b), Solar activity and hare dynamics—A cross-continental comparison, *Am. Nat.* **149**, 765–775.

Roland, J., and Taylor, P. D. (1997), Insect parasitoid species respond to forest structure at different spatial scales, *Nature* **386**, 710–713.

Ruxton, G. D. (1996), Dispersal and chaos in spatially structured models: An individual-level approach, *J. Anim. Ecol.* **65**, 161–169.

Ruxton, G. D., and Rohani, P. (1996), The consequences of stochasticity for self-organized spatial dynamics, persistence and coexistence in spatially extended host–parasitoid communities, *Proc. Roy. Soc. London Ser. B* **263**, 625–631.

Savill, N. J., and Hogeweg, P. (1997), Evolutionary stagnation due to pattern–pattern interactions in a co-evolutionary predator–prey model, *Artificial Life* **3**, 81–100.

Savill, N. J., and Hogeweg, P. (1998), Spatially induced speciation prevents extinction: The evolution of dispersal distance in oscillatory predator–prey models, *Proc. Roy. Soc. London Ser. B* **265**, 25–32.

Savill, N. J., Rohani, P., and Hogeweg, P. (1997), Self-reinforcing spatial patterns enslave evolution in a host–parasitoid system, *J. Theor. Biol.* **188**, 11–20.

Sherratt, J. A., Eagan, B. T., and Lewis, M. A. (1997), Oscillations and chaos behind predator–prey invasion: Mathematical artifact or ecological reality, *Phil. Trans. Roy. Soc. London Ser. B* **352**, 21–38.

Solé, R. V., and Valls, J. (1992), On structural stability and chaos in biological systems, *J. Theor. Biol.* **155**, 87–102.

Solé, R. V., Bascompte, J., and Valls, J. (1992), Stability and complexity of spatially extended two-species competition, *J. Theor. Biol.* **159**, 469–480.

Turing, A. M. (1952), The chemical basis for morphogenesis, *Phil. Trans. Roy. Soc. London* **237**, 37–72.

van der Laan, J. D., and Hogeweg, P. (1995), Predator–prey coevolution: Interactions across differenent time scales, *Proc. Roy. Soc. London Ser. B* **259**, 35–42.

Varley, G. C., and Gradwell, G. R. (1963), The interpretation of insect population changes, *Proc. Ceylon. Ass. Advmt. Sci.* **18**, 142–156.

Vilar, J. M. G., and Solé, R. V. (1998), Effects of noise in symmetric two-species competition, *Phys. Rev. Lett.* **80**, 4099–4102.

Wright, S. (1943), Isolation by distance, *Genetics* **28**, 139–156.